*Collection SFN* **12** (2011) 77–104

DOI: 10.1051/sfn/201112005

# Introduction to the density functional formalism and some illustrative applications to magnetism

M. Zbiri[1,*], M. Johnson[1], H. Schober[1], S. Rols[1], N. Qureshi[2], S. Clarke[3] and R. Mittal[4]

[1] *Institut Max von Laue-Paul Langevin, 6 rue Jules Horowitz, BP. 156, 38042 Grenoble Cedex 9, France*
[2] *II. Physikalisches Institut, Universität zu Köln, Zülpicher Strasse 77, 50937 Köln, Germany*
[3] *Department of Chemistry, Oxford University, Inorganic Chemistry Laboratory, Oxford, OX1 3QR, UK*
[4] *Solid State Physics Division, Bhabha Atomic Research Centre, Trombay, Mumbai 400 085, India*

**Abstract.** Some selected applications of spin-polarized density functional theory are presented to illustrate the robustness of the applied approaches to help interpretation and to ellucidate some observed, intriguing magnetic behavior, as highlighted by recent neutron scattering experiments. Both structure and dynamics are concerned through four examples covering the elastic and inelastic neutron scattering processes and dealing with the case studies of some complex transition metal containing inorganic materials. In the first two examples, molecular cluster calculations of the magnetic exchange coupling constant and the evaluation of the spin density distribution are shown. Further, periodic simulations of the magnetic bands and the spin-orbit coupling are introduced. Finally, the role of the magnetic interactions in the inelastic case is illustrated through investigating the corresponding effect on phonon dynamics relevant to superconductivity.

## 1. INTRODUCTION

The quest for new materials exhibiting attractive properties dedicated to fundamental research and/or to be used as a basis for developing industrially targeted practical applications has pushed the limit of the physico-chemical synthesis and fabrication to reach levels which were not attainable a couple of decades ago [1–3]. Usually, a given property is intimately related to the degree of complexity of the material subject of the probe. Studying complex materials with remarkable properties would become a challenging task without the help of simulations which provide the adequate tools to help designing new ways to achieve this goal [1]. Calculations through the implementation of a physically efficient theoretical models and numerically accurate algorithms are increasingly and widely adopted as necessary tools to help analysis and interpretation of the observations, and could be even used to drive a specific experiment (here the difference between measurement and experiment is to be considered). Furthermore in some cases, simulations are also used for the sake of prediction where experiments are not feasible or are dangerous to carry out [4]. Depending on the nature of the system, the type of the targeted property or characteristics, and the available computational ressources; calculations can mainly be done within three frameworks: empirical, semi-empirical and non-empirical. The latter which is also called ab-initio or from first principles – gathering together all those theoretical approaches which are

*e-mail: zbiri@ill.fr

mostly of a quantum-physical nature and are parameter-free (nothing to be adjusted or to be fitted to match observations!) [5].

Modern magnetism is based on the quantum origin of the magnetic interactions which are induced by the spin degrees of freedom. The spin as a quantum physical quantity, should be treated and described within this specific framework [6]. Neutrons are excellent probes when magnetism is concerned [7]. Indeed, since the neutron has a magnetic moment, it is scattered by the magnetic moments of the atoms in the sample leading to detailed information through the magnetic scattering. The latter which results from the dipole-dipole interaction between the magnetic moment of the neutron and the magnetic moment of an atom having unpaired electrons. Coherent elastic scattering can be used to determine the magnetic structure (i.e. the magnitude and orientation of magnetic moments in the structure), whereas the inelastic scattering can be used to measure the forces between magnetic moments (i.e. the strength of the exchange interactions). Solid theoretical foundations were built to treat accurately these features through an adequate description of the fascinating quantum nature of the spin. Such approaches can be incorporated into well established electronic structure formalisms; like the density functional theory (DFT) [5]. DFT has benefited from the huge progress made on the computing side on both the hardware and software levels allowing to apply the DFT-based ab initio model calculations to relatively large systems with enough accuracy to describe the role of the spin and its underlying physics [8].

Following a brief introduction to DFT highlighting how magnetism is handled, the aim of this article is to show, through some selected examples, how the DFT-based methods can be used to study some typical magnetic problems. The value of the following applications can be seen in the remarkable contribution of the ab initio simulations to provide explanations and to help investigating complex and intriguing magnetic behavior and properties in the presented case studies.

## 2. THE MANY-ELECTRON PROBLEM: FROM HARTREE TO DFT

### 2.1 The Hartree approach

One of the earliest attempts to solve the many-body problem [9] was made by Hartree [10]. He simplified the problem by making an assumption about the form of the many-electron wavefunction (wf), namely that it was just the product of a set of single-electron wfs. Having made this assumption it was possible to proceed using the variational principle [11, 12]

$$\psi(1,\ldots,N) = \varphi_1(1)\varphi_2(2)\cdots\varphi_N(N) \tag{2.1}$$

It follows that Hartree found the Hamiltonian equation of the many-electron system (or equation of motion). In fact, for an N-electron system there are N equations; one for each of the N single-electron wfs which made up the many-electron product wf. These equations turned out to look very much like the time-independent Schrödinger equation, except that the potential (the Hartree potential) was no longer coupled to the individual motions of all the other electrons, but instead depended simply on the time-averaged electron distribution of the atom [13].

### 2.2 The Hartree-Fock method: Including the exchange

Equation (2.1) is not antisymmetric, allowing the existence of unphysical states since the exchange effect of the electrons was not considered. But the Pauli principle can be fulfilled by constructing a trial wf which is entirely antisymmetric and by using the Slater determinant of one-particle states [14].

That is each electron is placed into another single-particle state as described by

$$\psi(1,2,\ldots,N) = \frac{1}{\sqrt{N!}}\begin{vmatrix} \varphi_1(1) & \cdots & \varphi_1(N) \\ \vdots & & \vdots \\ \varphi_N(1) & \cdots & \varphi_N(N) \end{vmatrix} \tag{2.2}$$

**Table 1.** Comparison of the scaling of the DFT against Hartree-Fock (HF), and some well established perturbative approaches (MP2 and MP4) and post Hartree-Fock methods (CCSD and QCISD).

| **DFT** | HF | MP2 | MP4 | CCSD(T) | QCISD(T) |
|---|---|---|---|---|---|
| $\mathbf{N^3}$ | $N^4$ | $N^5$ | $N^7$ | $N^7$ | $N^7$ |

This is the purpose of the Hartree-Fock (HF) method [10, 15]. All one-particle wfs are already orthonormal; i.e.$\langle \varphi_i \mid \varphi_j \rangle = \delta_{ij}$. Consequently, the HF equations can be derived and they contain an additional term not present in the Hartree's equations yielding the concept of an effective exchange charge not present in Hartree's theory. This term indicates the amplitude with which the electrons in states *i* and *j* can be found at positions **r** and **r'**, respectively.

### 2.3 The missing correlation in the HF theory

Mathematically, correlation means that two distribution functions are not independent of each other, but it does not imply causality. In many electron physics, two electrons are correlated if their spins are parallel. By convention the HF theory is said to have no correlation since it is a mean field, single particle description. The HF approximation results in a set of coupled single-particle equations which brought many important quantitative results to chemistry and physics. But this approximation fails in cases that require "chemical accuracy" of $\sim$1 kcal/mol and sometimes even qualitatively [4]. The missing term in the HF approach is the so-called "Coulomb correlation" or simply the correlation which energetically is the difference between the exact, non-relativistic calculation of the total energy and its HF counterpart:

$$E_{corr} \equiv E_0 - E_0^{HF} \tag{2.3}$$

Thus, the main error in the HF approximation originates from ignoring the correlated motion of each electron with every other. It is important to note that there are two types of correlation. The first one is called "dynamical" correlation because it refers to the dynamic character of the electron-electron interactions. The other kind of electron correlation is called "non-dynamical" or "static" correlation affecting the hole localization. Recovering this missing contribution and the need for an accurate and consistent treatment of electron correlation is one of the great challenges confronting electronic structure calculations in different domains. A number of "post-HF" methods have been developed to go beyond the mean-field approximation but that are not of much help in a computational efficiency sense to be applied to realistic and advanced materials. Other important formalisms that treat the correlation energy are quantum Monte Carlo (QMC) [16], electron propagator theory (EPT) [17], density-matrix renormalization group (DMRG) [18], and the density functional theory (DFT) which is our method of choice.

### 2.4 The Density Functional Theory

#### *2.4.1 Historical introduction*

DFT is a first principles method, its practical implementation combines a high efficiency with a relatively high accuracy. It uses the one-electron density, $\rho$, to describe a molecular (orbitals) or extended (bands) system. $\rho$ is a function of the three space coordinates only; i.e. $\rho = \rho(\mathbf{r})$ (or four degrees of freedom if the spin is taken into account). It is a quantity experimentally measurable by X-ray diffraction. Hence the complex mathematical object $\psi$ (wf) is replaced by the much simpler quantity $\rho$.

Table 1 compares the scaling of DFT to HF and some advanced perturbative approaches, and post HF methods. DFT offer the best scaling over the other methods. The good balance between the DFT scaling and its accuracy is the main reason behind its important and still growing success. The sequential development of DFT can be summarized as follows:

- The basic notion that the energy can be expressed in terms of density goes back to the Thomas-Fermi model (TFM) in 1927–1928 [19–22]. In this model, the ground state energy of a system moving in the external potential of a nuclear frame may be expressed directly and exclusively in terms of the electron density. However, the electron-electron interaction only takes account of the Coulombic effect ignoring the exchange and correlation contributions.
- Further improvement of TFM was made by Dirac [23] who added a term representing the exchange contribution to the TFM (TFDM model) [23]. But TFDM fails to describe chemical bonds and to predict the total energy for an atomic system [25].
- Few years after Dirac's improvement [23], von Weizsäcker [24] improved the TFDM to go beyond the atomic-like description of that model and therefore it would be possible to describe chemical bonds. He suggested to add a variation of $\rho$ to take account of its inhomogeneity via its gradient (TFDWM model). The TFDWM yields a "physical" meaning of the density close to the nucleus (finite entity), with correct asymptotic behavior (convergence).
- The first density-based scheme to be used for more than one atom was the HF-Slater, or $X_\alpha$, method [27–29]. Slater proposed that the effect leading to electron exchange and correlation energies can be given by a functional proportional to $\rho^{\frac{1}{3}}$. This is known as the $X_\alpha$ functional. He substituted the exchange part in the HF equations by $X_\alpha$ computed for uniform electron gas (UEG), using a method based on his augmented plane wave (APW) concept. This allows to speed up the calculations (exchange matrix elements calculation is avoided).
- In spite of these important successive refinements of "earlier" density functional models, solid foundations of DFT were provided in 1964 by Hohenberg and Kohn with their two fundamental theorems. In 1965 the major milestone in the development of DFT was introduced by Hohenberg, Kohn and Sham (HKS). They gave the proofs of these theorems by showing that DFT was an exact theory in the same sense as the wf theory [30].

### *2.4.2 The Hohenberg-Kohn-Sham formulation of DFT*

Following HKS, instead of using the full electronic wavefunction $\Psi_0(\{r_1\},\ldots,\{r_N\})$, the electronic ground state of a system can be entirely described by its electron density $\rho(r)$. The ground state density $\rho(r)$ of a many electron system in the presence of an external potential $v(r)$ uniquely determines the external potential (and $\Psi_0$). $\rho(r)$ is sufficient to construct the full Hamilton operator. Or, alternatively, by an auxilary electrons ($V_{ee}=0$) in an effective external potential $\hat{v}_{eff}=\hat{v}_s$, giving rise to the same density $\rho(r)$. The electron density $\rho(r)$ or the orbitals $\phi_1(\mathrm{r}),\ldots,\phi_N(\mathrm{r})$ are obtained by minimization of a density functional. Hence the existence of a total energy functional $\mathrm{E}[\rho(\mathbf{r})]$ and the problem can be solved via the variational principle. The information about the number of electrons can be easily obtained from the density itself

$$\int \rho(\mathbf{r})d\mathbf{r} = N \tag{2.4}$$

There is no exact way to systematically construct or obtain $\mathrm{E}[\rho]$. Consequently $\mathrm{E}[\rho]$ cannot be calculated without approximations. The usual procedure is to solve the Kohn-Sham (KS) equations [33] defined by

$$\left[-\frac{1}{2}\nabla^2+\hat{v}_S(\vec{r})\right]\phi_i(\vec{r})=\epsilon_i\phi_i(\vec{r}) \tag{2.5}$$

The first term in brackets is the kinetic energy operator

$$T_S[\rho(r)]=\sum_{i=1}^{N}\langle\phi_i|-\frac{1}{2}\nabla^2|\phi_i\rangle \tag{2.6}$$

which corresponds to kinetic energy of the reference system of N noninteracting electrons. The noninteracting reference system is a mono-determinantal wavefunction of the lowest N orbitals [34],

and leads to: (i) the exact density of the interacting system with v(**r**) as sum over densities over the occupied KS orbitals $\phi_i$,

$$\rho(r) = \sum_{i=1}^{N_{occ}} n_i |\phi_i(r)|^2 \tag{2.7}$$

and, (ii) the corresponding exact energy E[$\rho$(**r**)]. The KS potential accounts for all effects due to e-n and e-e interactions

$$\hat{v}_S(r) = v(r) + V_{Coul}(r) + \hat{v}_{xc}(r) \tag{2.8}$$

$v_S$(**r**) contains the attractive potential v(**r**) of the nuclei, the classical Coulomb repulsion $V_{Coul}$(**r**) within $\rho$(**r**), and also all exchange-correlation (XC) effects which are folded into a local potential $v_{xc}$(**r**). The latter is defined as the functional derivative of the XC energy $E_{xc}$ with respect to the density

$$v_{xc}(\mathbf{r}) = \frac{\delta E_{xc}[\rho(\mathbf{r})]}{\delta \rho(\mathbf{r})} \tag{2.9}$$

This is an effective one-electron formulation of the many-body problem, which is used in essence by most current implementations of DFT. The value of DFT can be seen in the accurate calculation of molecular and crystal properties, and also in the fact that DFT is rich in conceptual content [35, 36]. As far as magnetism is concerned, the XC contribution plays a predominant role on this regards.

However, the exact expression of $E_{xc}$ is not known. Thus, approximate formulas of $E_{xc}$ are needed. Several approximations have been developed: for example the local density approximation (LDA), or the semi-local DFT known as generalized gradient approximations (GGA). The total energy functional $E_{xc}[\rho]$ is often divided into two contributions, exchange term and correlation term

$$E_{xc}[\rho] = E_x[\rho(\mathbf{r})] + E_c[\rho(\mathbf{r})] \tag{2.10}$$

$E_x$ and $E_c$ depend differently on the density following a given approximation. One should note that the correlation part is more complicated to obtain than the exchange contribution. Many different approaches have been used to create improved XC functionals, and this yields an increasing number of the current developed functionals that can be recast into different classes: the LDA, the GGAs, the meta GGAs, and the hybrid ones. There are two main strategies for developing new functionals: (i) the first one is the semi-empirical way. In this approach, a flexible mathematical functional form is chosen depending on one or more parameters, and then fit these parameters to molecular experimental data; (ii) the second strategy is a "non-empirical" approach that follows the "Jacob's ladder" as presented by Perdew. In this approach, one considers that approximate functionals should be developed from first principles by incorporating known exact constraints, and thus if enough constraints are satisfied, all physical properties will come out correctly by themselves.

### *2.4.3 The Local Density Approximation (LDA)*

Within the UEG framework, the total XC energy can be written as [33]

$$E_{xc}^{LDA}[\rho] = \int \rho(\mathbf{r})(\varepsilon_x[\rho(\mathbf{r})] + \varepsilon_c[\rho(\mathbf{r})])d\mathbf{r} \tag{2.11}$$

where $\varepsilon_{xc}[\rho(\mathbf{r})]$ is the XC energy per particle

$$\varepsilon_{xc}[\rho] = \varepsilon_x[\rho] + \varepsilon_c[\rho] \tag{2.12}$$

The principle of LDA is to calculate $\varepsilon_x[\rho(\mathbf{r})]$ and $\varepsilon_c[\rho(\mathbf{r})]$ of the UEG as a function of $\rho$. From QMC [16] calculations, Ceperley and Alder evaluated the correlation functional [37]. Then, Vosko, Wilk and Nusair (VWN) [38] gave analytically the formula of $\varepsilon_c$ using a fit procedure. The success of LDA made the

popularity of modern DFT. However for a better treatment of inhomogeneous systems such as the molecular materials, functionals with other forms of the density dependence are needed.

### *2.4.4 The Generalized Gradient Approximation (GGA)*

In their original papers, HK [30] and KS [33] presented a gradient expansion approximation (GEA) based on the polarizability of the homogeneous electron gas. But it was already shown that the GEA has a range of validity, which is limited to slowly varying systems. Furthermore, the GEA exchange hole is not strictly non-positive, and does not integrate to $-1$ as it should [43], which is one of the main reasons behind the development of the gradient corrections. Becke's way to build model functionals, which is primarily adopted to develop GGA, can be qualified as a semi-empirical way for the design of functionals [44–47]. The second idea is advocated by Perdew, he states that the development of XC functionals should be based on first principles derived from quantum mechanics [48–51].

In GGA, the gradient $\nabla\rho$ is included as the only new variable, and one tries to determine the best scheme that fulfills the relation:

$$E_{xc}^{GGA}[\rho_\alpha, \rho_\beta] = \int f(\rho_\alpha(\mathbf{r}), \rho_\beta(\mathbf{r}), \nabla\rho_\alpha(\mathbf{r}), \nabla\rho_\beta(\mathbf{r}))d\mathbf{r} \tag{2.13}$$

A good example of a gradient corrected correlation functional is the famous and popular LYP (Lee-Yang-Parr) functional [55]. Contrary to the other functionals, LYP is not derived from an UEG model. Indeed, based on the work of Colle and Salvetti [56] and from a correlated wf for a two electron system [57], Lee, Yang and Parr derived the LYP correlation expression [55]. Further, we can cite important functionals which are widely adopted and do not contain adjustable parameters like PW91 (Perdew and Wang) [50, 51] and PBE (Perdew, Burke and Erzenhof) [54].

### *2.4.5 Some limitations and towards significant improvements*

Like any other approximative method, "standard" DFT functionals fail badly in some certain cases, especially for the treatment of strongly correlated magnetic systems:

- Spin polarization: although KS-DFT yields good results for the low density limit (spin-compensated) case, doing a many-body perturbation expansion [52] and/or treating correctly open-shell systems (partially filled d- or f-levels) require spin-dependent functionals [39]. The spin-dependence (magnetic interactions, magnetic field, relativistic effects) has to be taken into account via the so-called spin-polarized DFT [40–42]. This is done by separating explicitly the contributions of the spin-up and spin-down components of the polarized electron density and its dependencies (gradient, Laplacien, ...)

$$E_{xc}[\rho] = \int f(\rho^\uparrow(\mathbf{r}), \rho^\downarrow(\mathbf{r}), \nabla\rho^\uparrow(\mathbf{r}), \nabla\rho^\downarrow(\mathbf{r}), \ldots, \ldots)d\mathbf{r} \tag{2.14}$$

Hence the spin densities of both spin components are defined as

$$\rho^\uparrow(\vec{r}) = \sum_{i=1}^{N_{occ}^\uparrow} n_i^\uparrow |\phi_i^\uparrow(\vec{r})|^2 \qquad \rho^\downarrow(\vec{r}) = \sum_{i=1}^{N_{occ}^\downarrow} n_i^\downarrow |\phi_i^\downarrow(\vec{r})|^2 \tag{2.15}$$

The total electron density satisfies

$$\rho = \rho^\uparrow + \rho^\downarrow \tag{2.16}$$

Interestingly, the magnetization density or the excess magnetization can be written as

$$m = \rho^\uparrow - \rho^\downarrow \tag{2.17}$$

This an important quantity when evaluating the magnetic moment or simulating the spin (distribution) density map over the magnetic sites of a given material.

- The self interaction error: LDA and GGA are not self-interaction free. Indeed, the e-e Coulomb part $V_{Coul}$ contains the (spurious) interaction of an electron with itself

$$\sum_{i=1}^{N} \frac{1}{2} \int \int \frac{|\phi_i(\vec{r})|^2 \phi_i(\vec{r}')|^2}{|r - r'|} d^3 r d^3 r' \tag{2.18}$$

This contribution can be removed by the exchange energy $E_x$. Therfore the HF theory is self-interaction free

$$V_{ee} + E_x = 0 \tag{2.19}$$

In DFT this issue can be solved by adopting some – partially – self-interaction free or corrected methods:

- Including the HF exact exchange leading to the well known hybrid DFT. This approach is very adequate to describe the magnetic interactions and the related properties, especially in the molecular crystals/systems. We adopt it for the studies presented in the first two applications in Section 3 and Section 4. The concept of the hybrid DFT is introduced hereafter.
- Correcting the balance between the on-site (for a given angular momentum and atom type) and the hopping contributions following the characteristics of the materials and by introducing explicitly two parameters U (Coulomb repulsion) and J (hopping term) via the Hubbard model into the KS equations. This is the purpose of the DFT+U method and it is used for the third application in Section 5.
- Considering some self-interaction corrected functionals, e.g. Perdew and Zunger.

### *2.4.6 The hybrid functionals*

In practice, in order to get the closest possible functional to the exact universal one (even for the moment, there is no hope of writing down that exact functional), one has to expand the list of the local ingredients of a functional $E_{xc}[\rho_\alpha, \rho_\beta]$ beyond the electron density to include other "exact" and accurate quantities (Jacob's ladder concept from Perdew's view). Within this spirit, and since the exchange contribution is more important (in absolute value) than that of the correlation, the performance of the density functionals (DF) can be significatively improved by improving the exchange functionals. One can do better, the exchange HF energy is "exact"! thus it can be combined with the "standard" DFT yielding the hybrid HF-DFT approaches.

The best way to build "accurate" hybrid density functionals (HDF) is to use the adiabatic connection concept [60, 61]. In this approach, a parameter $\lambda$ is introduced to tune the electron-electron interaction for a given system by taking a sum of fictitious systems all with density $\rho$ and different e-e interaction,

$$E_{xc} = \int_0^1 E_{xc,\lambda} d\lambda \tag{2.20}$$

$\lambda = 0$ corresponds to non-interacting electrons,

$$E_{xc,\lambda=0} = E_X = F_{HF} \tag{2.21}$$

$\lambda = 1$ corresponds to full interacting electrons,

$$E_{xc,\lambda=1} = E_{xc} + T - T_S \tag{2.22}$$

In the equation (2.20), the adiabatic parameter $\lambda$ has two extreme values *0* and *1* corresponding to equation (2.21) and equation (2.22). But the difficulty arises when $\lambda$ varies between these two values. However, one can overcome this problem by writing the XC energy as a linear expansion with respect

to $\lambda$. The Becke "Half&Half" functional [62] is then given by

$$E_{xc}^{HH} = \frac{1}{2}E_{xc}^{\lambda=0} + \frac{1}{2}E_{xc}^{\lambda=1} \tag{2.23}$$

where $E_{xc}^{\lambda=0} = E_x^{Exact} = E_x^{HF}$, and the LDA functional for $E_{xc}^{\lambda=1}$ was used to represent the DF part of equation 2.23. The "Half&Half" HDF was improved by using three semi-empirical parameters in order to make a weighting of the different contributions [63],

$$E_{xc}^{B3} = E_{xc}^{LSD} + a(E_{xc}^{\lambda=0} + E_X^{LSD}) + bE_X^{B88} + cE_C^{PW91} \tag{2.24}$$

where $a$, $b$, and $c$ are semiempirical coefficients determined by an appropriate fit to the experimental data. $E_{xc}^{\lambda=0}$ is the exact exchange energy (tuned by $a$), $E_X^B$ is Becke's 1988 gradient correction (to the LSDA) for exchange [53], and $E_C^{PW91}$ is the 1991 gradient correction for correlation of Perdew and Wang [64–66]. When the functional PW91 is replaced by the LYP [55] one for the correlation part, one obtains the very popular B3LYP [67] used hereafter in Section 3 and Section 4. B3LYP contains the same three semiempirical parameters, but with the following expansion

$$E_{xc}^{B3LYP} = (1-a)E_{xc}^{LSD} + aE_{xc}^{\lambda=0} + bE_X^{B88} + cE_C^{LYP} + (1-c)E_C^{LSD} \tag{2.25}$$

Above, a second strategy to build a new functional has been introduced, namely the non-parametric way. In this case, the hybrid functional is written with respect to $\lambda$ as follow:

$$E_{xc,HDF}^{\lambda}(n) = E_{xc,DF}^{\lambda} + (E_{X,HF} - E_{X,DF})(1-\lambda)^{n-1} \tag{2.26}$$

where $n \geq 1$ is an integer to be determined, controlling how rapidly the correction to the DF vanishes as $\lambda \to 1$. Then

$$E_{xc,HDF} = \int_0^1 d\lambda E_{xc,HDF}^{\lambda} = E_{xc,DF} + \frac{1}{n}(E_{X,HF} - E_{X,DF}) \tag{2.27}$$

The optimum integer $n$ should be the lowest order [69] of perturbation theory which provides a realistic description of the shape or $\lambda$-dependence of the exact $E_{xc}^{\lambda}$

$$E_{xc}^{\lambda} \approx (c_0 + c_1\lambda + \cdots + c_{n-1}\lambda^{n-1}); \quad (0 \leq \lambda \leq 1) \tag{2.28}$$

This choice maximizes the similarity of $E_{xc,HDF}^{\lambda}$ to $E_{xc,DF}^{\lambda}$ near $\lambda = 1$, while ensuring that no unnecessary powers of $\lambda$ are introduced into Eq. (2.26). The $E_{xc,HDF}^{\lambda=1}$ and $E_{xc,DF}^{\lambda=1}$ can each be fitted accurately by a polynomial like Eq. (2.28), with an index $n$ no higher than that needed for an accurate representation of the exact $E_{xc}^{\lambda}$. An ideal hybrid functional would be sophisticated enough to optimize n for each system and property, but the accuracy of MP4 (fourth-order Møller-Plesset perturbation theory) [72] for most molecules suggests $n = 4$ as the best single choice

$$E_{xc}^{HDF}(n=4) = E_{xc}^{DF} + \frac{1}{4}(E_X^{HF} + E_X^{DF}) \tag{2.29}$$

The PBE0 hybrid functional [69, 70] is a good example of a hybrid model without adjustable parameters. The idea is to use the pure GGA PBE [54], and to add 25% of the HF exchange to it based on purely theoretical and physical considerations. Thus PBE0 is a variant obtained inserting the PBE XC functional into eq. (2.29) leading to

$$E_{xc}^{PBE0} = E_{xc}^{PBE} + 0.25(E_X^{HF} + E_X^{PBE}) \tag{2.30}$$

It has been found recently that PBE0 performs nicely when the magnetic and structural properties are concerned. To some extent it shows also a good performance when describing some optical characteristics.

Figure 1 summarizes the characteristics and the successive improvements made and being pursued towards building an accurate and universal density-based approach. Non-local functionals which

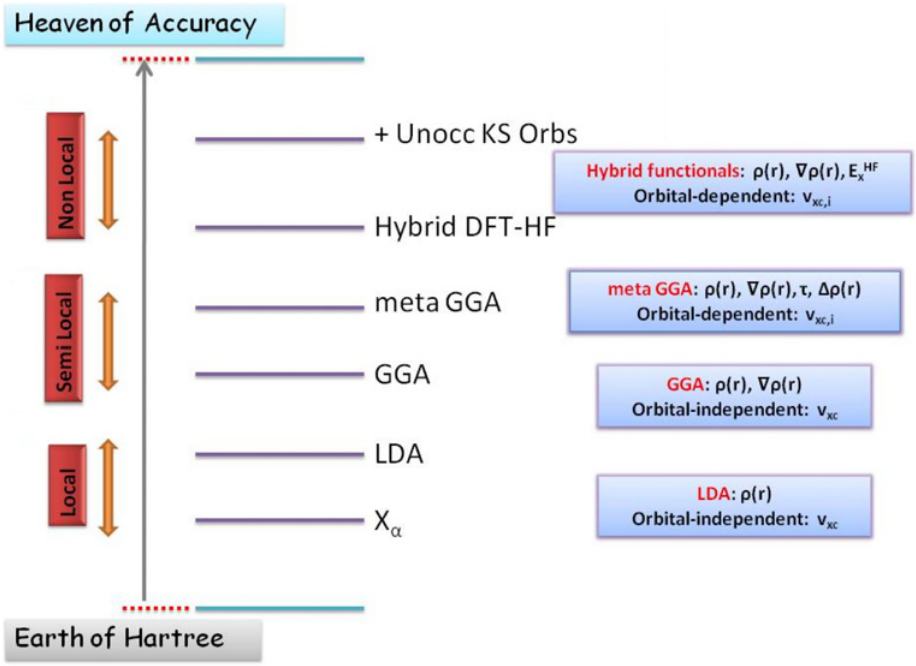


**Figure 1.** Schematic illustration of the Perdew's view of the hierarchy of DFT approximations. It is pictured as "Jacob's ladder" rising from the "Hartree world" to the "chemical accuracy heaven" [58, 59].

are orbital-dependent and which are either meta (dependence on the kinetic energy of the electron density), hybrid (as explained above) or of both natures (as recently applied successfully to the crucial case of the weak molecular interactions by describing the dispersion forces) are nowdays used for different applications [71, 81]. As far as magnetism is concerned, current DFT methods, determining spin populations (up and down) and their distribution, provide an adequate framework and lead to satisfactory results regarding the increasing complexity of the studied materials. In the followings some applications are presented where some anoumalous magnetic behaviors were explored or where the role of magnetism is highlighted withing the DFT framework.

## 3. MAGNETIC EXCHANGE COUPLING CONSTANT

Bridged, binuclear transition metal containing, inorganic molecular crystals are good frameworks to study the exchange interactions and its underlying mechanisms. The versatile azide group $N_3^-$ can be used as a bridging ligand between the magnetic centres [82]. It was assumed, following some geometrical rules [83–85], that the end-on azido bridged complexes – in contrast to the end-to-end case – show ferromagnetic coupling (Figure 2 shows both types). Here we report on some DFT-rationalized case studies where this is violated.

The magnetic exchange coupling constant is evaluated for a set of five end-on azido-bridget Cu(+II) complexes. Four of them exhibit unusual/unexpected antiferromagnetic (AF) ordering ($J < 0$) and are labeled C1 to C4, whereas the fifth one – labeled C5 – is a "normal" ferromagnet ($J > 0$). The latter is investigated for the sake of reliability of the model calculations. The broken symmetry approach within the hybrid DFT framework is applied to suitably representative molecular magnetic units extracted from the corresponding crystal structures [86].

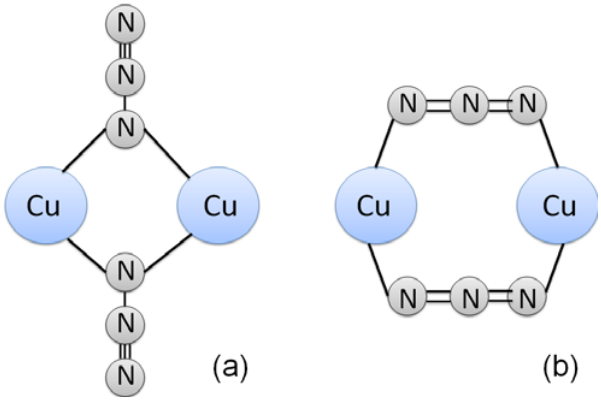


**Figure 2.** Schematic illustration of the two possibilities to build a Cu-Cu azide bridge: (a) the end-on case (the present case) and (b) the end-to-end case.

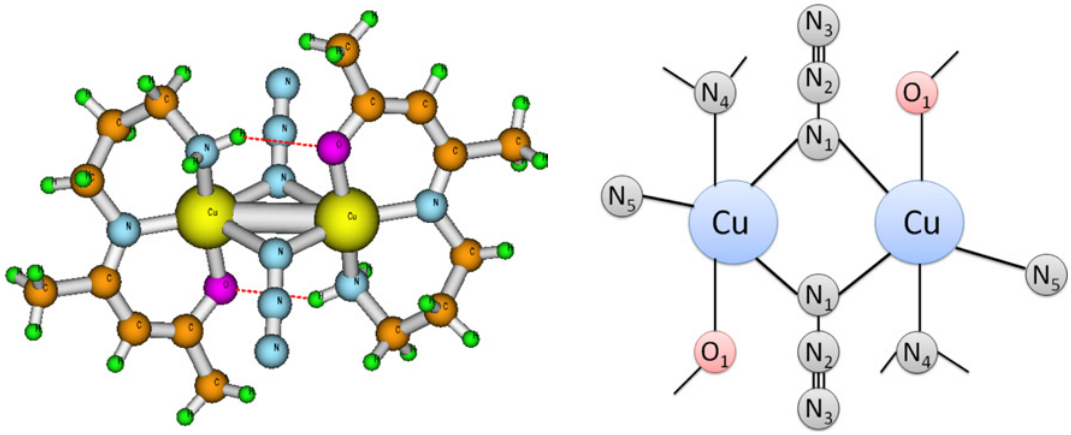


**Figure 3.** Left: Schematic illustration of one of the studied azido-bridged complexes. The remaining four systems having very similar tridentate Schiff base blocking ligands. Right: Labeling of the relevant neighbouring of the Copper cations to facilitate assignement of data in Table 3.

The magnetic interaction between the two paramagnetic centres Cu(II)[$d^9$] with local spin operators $\vec{S}_1$ and $\vec{S}_2$ can be described adopting the Heisenberg-Dirac-van-Vleck spin Hamiltonian [87–91]

$$H_{HDVV} = -J\vec{S}_1.\vec{S}_2 \tag{3.1}$$

The broken symmetry (BS) formalism proposed by Noodlemann and coworkers [92–94] is accessible through the DFT framework and has been successfully applied earlier to rationalize the magnetic behavior of several transition metal complexes [95–102]. The BS single determinant is the spin polarized solution of the KS equations for the singlet state using different spatial orbital for different spins [103].

For the present systems with two interacting unpaired electrons on the magnetic centres Cu(II)[$d^9$], the coupling constant J or the singlet-triplet gap can be defined by a general expression with non spin-projected energy ($S_2 \leq S_1$)

$$J = \frac{(E_{BS} - E_{HS})}{2S_1S_2 + S_2} \tag{3.2}$$

$E_{BS}$ and $E_{HS}$ are the energies of the BS state and High-spin (HS) state, respectively. Equation (3.2) corresponds to the non-spin projected energy. Another expression of J as a function of BS and HS energies can be obtained assuming only that the singly occupied molecular orbitals (SOMO) are orthogonal. Noodlemann [104] referred to this approximation as the weak bonding regime. In the case that the orthogonality is generalized and considering the present systems having one unpaired electron per magnetic site ($S_1 = S_2$ and $S = S_1 + S_2$), $J$ is given by

$$J = E_{BS} - E_{HS} \tag{3.3}$$

meaning that the spin-orbitals of the magnetic centers are fully localized. This procedure does not account for reduced spin contamination in species with diminished diradical character. To project out those triplet states which contaminate the BS solutions, corrections based on the spin projected method [105, 106] can be included leading to

$$J = \frac{2(E_{BS} - E_{HS})}{\langle S^2\rangle_{HS} - \langle S^2\rangle_{BS}} \tag{3.4}$$

The expectation value $\langle S^2\rangle$ is calculated using [107]

$$\langle S^2\rangle = \langle S^2\rangle_{exact} + N^{\beta} - \sum_{i}^{N}\sum_{j}^{N} |\, S_{ij}^{\alpha\beta}\,|^2$$

with: $\langle S^2\rangle_{exact} = [\frac{N^{\alpha}-N^{\beta}}{2}][\frac{N^{\alpha}-N^{\beta}}{2}+1]$ and $S_{ij}$ is the overlap integral of $\alpha$-orbital $i$ with $\beta$-orbital $j$. $N$ is the number of electrons where $N^{\alpha} \geq N^{\beta}$.

The calculations were carried out using the Amsterdam Density Functional (ADF) package [80] using the B3LYP hybrid XC functional [67]. The experimentally determined geometries from X-ray diffraction were used for the calculations. Because a small variation in the geometry can have a big effect on the calculated magnetic interaction parameters [97], neither variation of the geometrical parameters nor structural relaxation were attempted. To study the effect of the functional (LDA, GGA, etc.), "standard" DFT calculations are firstly carried out employing equation (3.3). GGA leads to positive values of the calculated exchange magnetic coupling constants for the four complexes (ferromagnetic interaction). Thus the magnetic interaction is well described only for the ferromagnetic compound (C5) having $J_{exp} = 2.9\,cm^{-1}$. Computationally, the following values are obtained 2.7, 2.55 and 3.01 $cm^{-1}$ using the XC functionals PW91, BLYP and BP, respectively.

Non-hybrid DFT functionals can describe correctly the ferromagnetic interaction (compound C5), but fails to reproduce the observed AF interaction (compounds C1-C4). On the other hand HF calculations predicted negative values of $J$ for all the five compounds, which is also not accurate since $J$ for C5 should have a positive value.

It is well established that the specific combination of the HF exchange and DFT within the B3LYP hybrid functional [67] offers a good description of both the BS and the HS states. Indeed, in earlier works this has led for different case studies to calculated exchange coupling constants which are in a good agreement with the experiments [97–99, 108]. We have adopted therefore B3LYP. Both Equation (3.3) (non-spin projected) and Equation (3.4) (spin-projected) are used. Results of the calculations are gathered in Table 2. with the experimental data. From the calculations we notice that the BS and HS states are well localized, i.e., $\langle S^2\rangle_{BS} \simeq 1$ and $\langle S^2\rangle_{HS} \simeq 2$. That is due to the strong localization of the wavefunction at the metal centres and given the very small experimental value of $J$, the spin-projected and non-spin projected techniques produce closely similar results that are in a remarkable agreement, both in the sign and in the magnitude, with the experimental data.

Further, details of the spin density distribution in all the complexes are extracted from the hybrid DFT calculations [86]. The atomic Mulliken spin population in the coordination sphere of each copper(II) including the metal cation itself is obtained. This type of calculation was successfully implemented in other $\mu_{1,1}$-azido copper(II) dimers earlier to understand the spin polarization mechanism

**Table 2.** Comparison of calculated exchange coupling constants ($cm^{-1}$) for the five complexes, using non-spin projected (Eq. 3.3) or spin-projected (Eq. 3.4) methods, and experimental results [86]. Expectation values of total square spin operators for both broken symmetry (BS) and high spin (HS) states, used for Eq. 3.4, are shown. All the compounds have same core structure, $[Cu_2L_2(\mu_{1,1}-N_3)_2]$. $LH_2$ for 1 is N-(3-aminopropyl)-salicylaldimine, for 2 is 7-amino-4-methyl-5-azahept-3-en-2-one, for 3 is 8-amino-4-methyl-5-azaoct-3-en-2-one and for 4 is 1-(N-salicylideneiimino)-2-aminoethane.

| | $\langle S^2\rangle_{BS}$ | $\langle S^2\rangle_{HS}$ | $J$ (Eq. (3.3)) | $J$ (Eq. (3.4)) | $J_{Exp}$ |
|---|---|---|---|---|---|
| C1 | 1.0036 | 2.0035 | −3.31 | −6.62 | −1.8 |
| C2 | 1.0028 | 2.0030 | −1.28 | −2.56 | −3.1 |
| C3 | 1.0040 | 2.0039 | −4.54 | −9.08 | −8.5 |
| C4 | 1.0035 | 2.0036 | −3.36 | −6.72 | −4.2 |
| C5 | 1.0045 | 2.0043 | 4.17 | 8.34 | 2.9 |

**Table 3.** Calculated Mulliken spin populations in the triplet state (HS state) [86]. The atomic assignement is provided in Figure 3.

| | C1 | C2 | C3 | C4 | C5 |
|---|---|---|---|---|---|
| Cu1 | +0.52 | +0.53 | +0.52 | +0.52 | +0.52 |
| N1 | +0.076 | +0.069 | +0.081 | +0.074 | +0.08 |
| N2 | −0.008 | −0.005 | −0.009 | −0.001 | −0.007 |
| N3 | +0.098 | +0.081 | +0.11 | +0.11 | +0.1 |
| N4 | +0.098 | +0.01 | +0.09 | +0.09 | +0.08 |
| N5 | +0.1 | +0.1 | +0.08 | +0.09 | +0.09 |
| O1 | +0.11 | +0.12 | +0.13 | +0.13 | +0.13 |

and the delocalization of the unpaired electrons of metal centers [95]. Table 3 gathers the calculated Mulliken spin densities for the triplet state. Our results convincingly demonstrate that there is a relative delocalization of the unpaired electron on Cu(II). Small positive values of spin density on the bridging and terminal nitrogen atoms ($N_1$ and $N_3$) of the azide group as well as on the other coordinated atoms ($N_4$, $N_5$ and $O_1$). Interestingly, a remarkable negative contribution is found on the central nitrogen atoms ($N_2$) of the $N_3^-$ bridge. This is in excellent agreement with other reports available in the litterature and compares nicely with data of Polarized Neutron Diffraction (PND) [95, 96, 109]. The sign alternation of the spin density at the $N_1$ and $N_2$ atoms of the azido-bridge is consistent with spin polarization by the bridging nitrogen atoms and it highlights the superexchange pathway between the two magnetic cations.

## 4. SPIN DENSITY DISTRIBUTION

This application is aimed at investigating the anomalous magnetization distribution in the Kagome staircase compound $Co_3V_2O_8$ representing the 3d transition metal ortho-oxo-vanadates [110, 111].

The crystal structure (Figure 4), having two inequivalent cobalt sites $Co_c$ (cross-tie) and $Co_s$ (spine), is characterized by edge-sharing $CoO_6$ octahedra forming buckled layers of corner-sharing triangles (the kagome staircases) which are separated along the $b$ axis by $VO_4$ tetrahedra.

The ferromagnetic structure ($T < 6.2$ K) reveals two significantly different zero-field magnetic moments for the two cations $Co_c$ and $Co_s$ ions of 1.54 and 2.73$\mu_B$, respectively [112]. Interestingly, both the ions present high-spin configurations as the macroscopic measurements exhibit a saturation of the $Co_c$ moments [113].

Investigating the magnetization density, which is reflected by the respective magnetic form factors of the ions, can reveal preferred exchange pathways with the presence of magnetization on the neighbouring oxygen and vanadium sites. Induced magnetization on the empty d-shell of V sites would

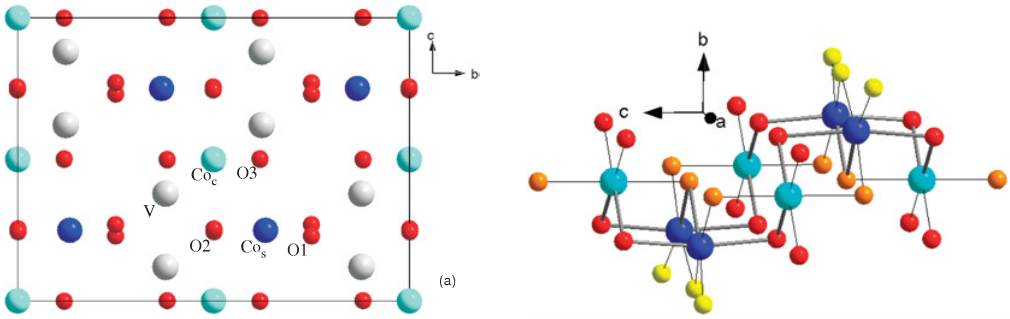


**Figure 4.** Left: The crystal structure of $Co_3V_2O_8$ viewed along the a-axis showing the crystallographically inequivalent atoms (2 cobalts, 3 oxygens and 1 vanadium). Right: molecular view involving the Cobalt cations and the Oxygen anions in two octahedral building blocks which are modelled separately using the quantum chemical molecular cluster calculations to get the non-empirical magnetic form factors [114].

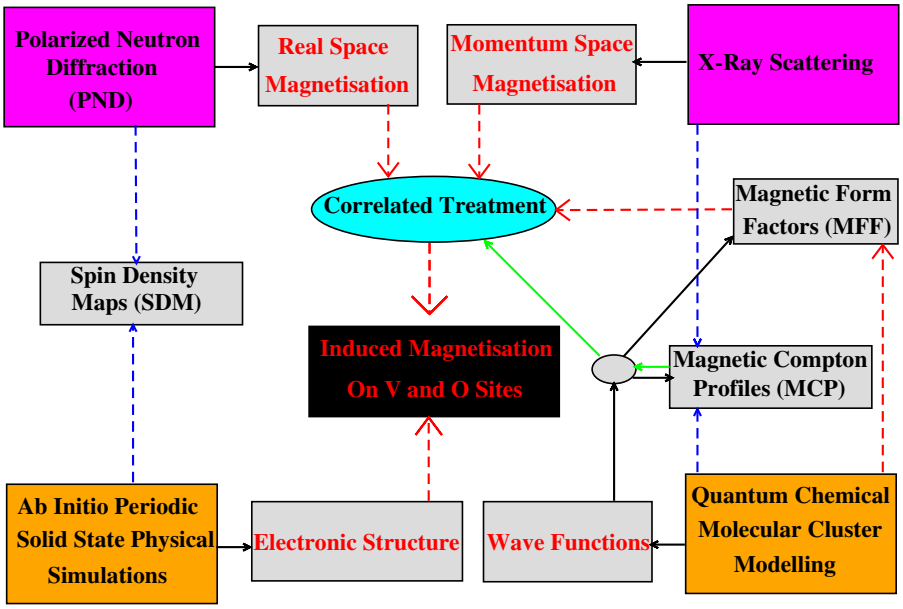


**Figure 5.** Illustration of the procedure [114] combining the DFT-based ab initio simulations (single molecule and periodic), polarized neutron diffraction and X-ray scattering to shed light on the observed anoumalous magnetization distribution in the Kagome staircase $Co_3V_2O_8$.

allow interlayer coupling by super-superexchange. Polarized neutron diffraction (PND) and magnetic Compton scattering (MCS) experiments have been carried out giving the spin density in real space and the magnetization density in momentum space, respectively. The population of each spin-orbital must be represented likewise in the observed densities in both spaces. Precise analysis of these quantities is required in order to determine the exact contribution of the atomic species and to elucidate the density distribution of the unpaired magnetic electrons and their interaction. This is where the present spin-polarized DFT calculations complement synergistically the experiments [114].

Ab-initio spin-polarised molecular cluster calculations were performed to extract the molecular orbitals (MOs) and to proceed with the correlated refinement of both PND and MCS techniques following the scheme shown in Figure 6. Two different clusters $Co_{cO_6}$ and $Co_{sO_6}$ (Figure 4 – right panel)

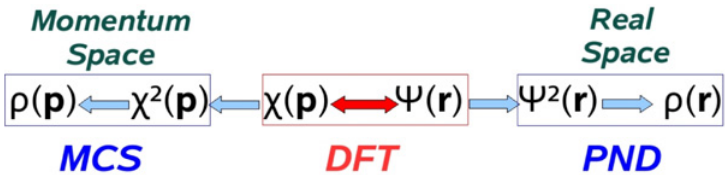


**Figure 6.** From Hybrid DFT calculated molecular orbital coefficients (MOs), the real space density $\rho(\mathbf{r})$ and the momentum space density $\rho(\mathbf{p})$ can be deduced. The latter which involves a Fourier transformation of the MOs [114].

were chosen and modelled separately. The calculations were performed using the quantum chemical GAMESS program [115]. The functional B3LYP was employed to approximate the XC interaction [67]. In order to mimic the Madelung potential of the crystal, the two quantum mechanical clusters were surrounded by point charges (PC) according to the effective fragment potential method [116]. Therefore a 1565 PC grid representing a $3 \times 3 \times 3$ super-cell, centered around the respective Co ions, has been built. The MO coefficients relevant to the 3d-shell of each cobalt cation were extracted from the simulations and used to model the magnetic Compton profiles (MCP) and the magnetic form factors.

MCP measures the 1D momentum space projection of $\rho_{mag}(\mathbf{p})$ of the spin polarised electrons

$$J_{mag}(p_z) = \int\int [\rho^{\uparrow}(\vec{p}) - \rho^{\downarrow}(\vec{p})] dp_x dp_y \qquad \mu_{spin} = \int J_{mag}(p_z) dp_z \tag{4.1}$$

Further, periodic calculations using the Vienna ab-initio simulation package (VASP) [117, 118] were carried out for the extended system to simulate the spin density map and to extract the electron density of states, allowing a direct evaluation of the induced magnetization on the oxygen and vanadium sites. The Hubbard correction has been applied with different settings of the on-site (U) and hopping (J) parameters within the Dudarev's scheme [119, 120].

The nuclear structure factors, deduced from the unpolarized neutron experiments, have been used to derive the magnetic structure factors from the observed flipping ratios. As the crystal structure is centrosymmetric the experimental magnetization density can be directly reconstructed by Fourier synthesis. Figure 7 (upper panel) highlights the good agreement between the observed and DFT simulated magnetization density in the real space, projected onto the *b*-*c* plane. Despite the fact that a field of 2 T has been applied along the easy axis *a* for the flipping ratio measurement, the magnetic moments of $Co_s$ and $Co_c$ are still significantly different.

Remarkable induced magnetization can be observed experimentally and computationally on the V and O sites. The real space quantities have simultaneously been refined with the momentum space quantities as the spin-orbitals contribute to both densities in the same way. MCPs provide the one-dimensional projection of the momentum spin density, as shown in Figure 7 (lower panel), and the shape of these profiles makes it possible to determine the population of each orbital. In real space this is represented by the magnetic form factor. The correlated refinement yielded stable and reliable results. The sum of the individual magnetic moments [$\mu(Co_c) = 1.54\,\mu_B$, $\mu(Co_s) = 2.87\,\mu_B$, $\mu(V) = 0.41\,\mu_B$, $\mu(O_1) = 0.05\,\mu_B$, $\mu(O_2) = 0.35\,\mu_B$, $\mu(O_3) = 0.36\,\mu_B$] with respect to their site multiplicity leads to a value of 3.52 $\mu_B$, which is in good agreement with macroscopic measurements [113], where the magnetic moment has only been attributed to the Co cations [112]. Our study, however, shows that spin populations are equally distributed over the $t_{2g}$ and $e_g$ levels for $Co_s$, but that only 30% of the magnetic signal stems from the $e_g$ orbitals for $Co_c$. Covalency is therefore at the origin of this reduced value with the relatively large induced moments on $O_2$ and $O_3$ anions surrounding $Co_c$.

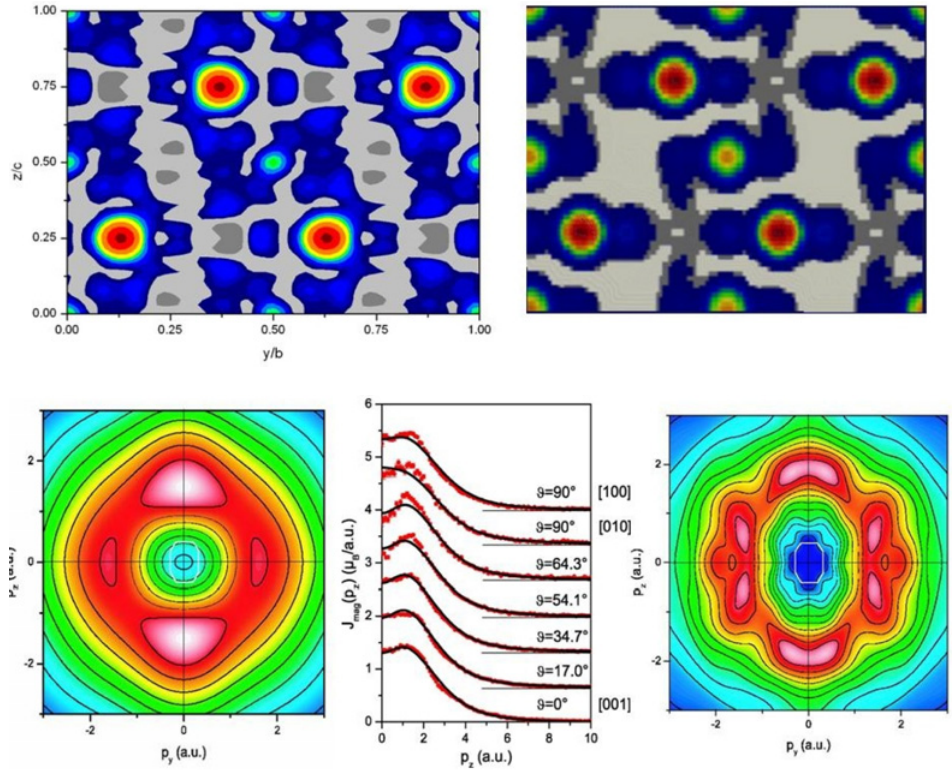


**Figure 7.** Top panel: observed (left) and simulated (right) spin density map in real space. Bottom panel: Reconstructed, experimental (left) and modelled (right) spin density in momentum space. The middle figure compares the corresponding observed (dots) and simulated (solid curves) magnetic Compton profiles [114].

## 5. MAGNETIC BANDS AND SPIN-ORBIT COUPLING

The layered oxysulfides $(Sr_{1-x}Ba_x)_2CoO_2Cu_2S_2$ $(0 \leq x \geq 1)$ offer high symmetry structures with the cobalt ion in strictly planar oxide layers, and this is irrespective of the nature of the alkaline earth cation (Sr or Ba) or even the chalcogenide anion. Their antiferromagnetic (AF) structures have been determined by powder neutron diffraction [121]. The magnetic reflections present in the diffraction patterns can in all cases be indexed using a $\sqrt{a} \times \sqrt{a} \times c$ expansion of the nuclear cell (Figure 8).

The nearest neighbor $Co^{2+}$ moments couple antiferromagnetically within the square planar $CoO_2$ layers. The ordered magnetic moment of $Co^{2+}$ in $Sr_2CoO_2Cu_2S_2$ $(x = 0)$ is 3.8(1) $\mu_B$ at 5 K, consistent with the high spin $Co^{2+}$ ions carrying three unpaired electrons (weak field coupling scheme) and with an additional significant unquenched orbital component. The ordered moment in $(Sr_{1-x}Ba_x)_2CoO_2Cu_2S_2$ increases with increasing Ba content, and a structural distortion from the tetragonal symmetry I4/mmm $(x = 0)$ to the orthorhombic one Immm $(x = 1)$ occurs. In $Ba_2CoO_2Cu_2S_2$ $(x = 1)$, having $Co^{2+}$ in an extremely square planar environment, an ordered moment of 4.5(1) $\mu_B$ has been refined at 5 K, which is over $0.7\mu_B$ larger than that in $Sr_2CoO_2Cu_2S_2$. Thus the unquenched orbital component in this case is even larger than that observed in octahedral $Co^{2+}$ systems such as CoO, suggesting hence an orbital contribution to the observed total magnetic moment. Ab initio simulations are needed to explore the electronic structure of the magnetic d-levels and the nature of the d-d interactions of the magnetic cations in $Sr_2CoO_2Cu_2S_2$ and $Ba_2CoO_2Cu_2S_2$. Spin polarisation, strong electron correlation and non-collinear effects have to be considered within the applied framework. DFT-based first-principles

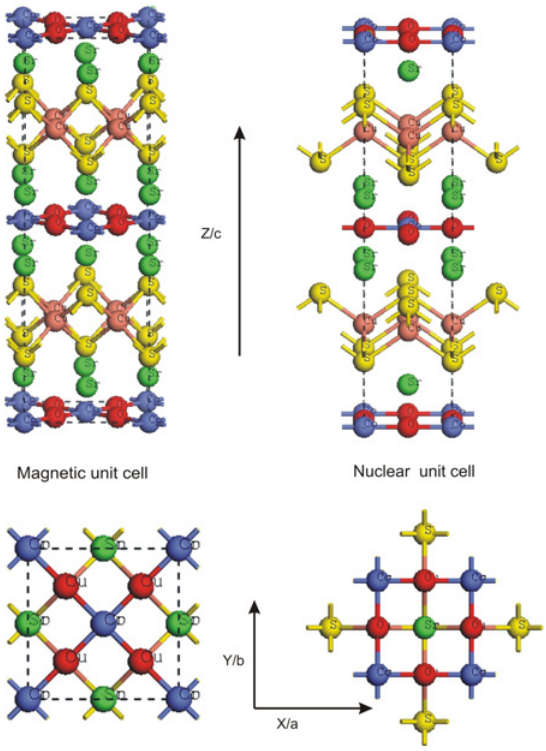


**Figure 8.** Schematic illustrations of the nuclear and magnetic structures of the oxy-chalcogenides $A_2CoO_2Cu_2S_2$ with $A = \{Sr, Ba\}$.

**Table 4.** Stabilization energies of the observed AF ground state against the non-magnetic state (NM) and a reference ferromagnetic phase (F). Different values of the on-site Coulomb term in the range 1–4 eV have been used. The terms $U_2$, $U_3$ and $U_4$ refer to the values 2, 3 and 4 eV, respectively. Optimal results are obtained with a correction of 3 eV, therefore only the results corresponding to $U_3$ are shown.

| $\Delta E$ (eV) | **Sr**$CoO_2Cu_2S_2$ | **Ba**$CoO_2Cu_2S_2$ |
|---|---|---|
| $\lvert E_F\rvert - \lvert E_{NM}\rvert$ | 1.46 | 1.70 |
| $\lvert E_{AF}\rvert - \lvert E_{NM}\rvert$ | 0.93 | 0.96 |
| $\lvert E_{AF}\rvert - \lvert E_F\rvert$ | −0.53 | −0.74 |
| $\lvert E_{AF\text{-}U_2}\rvert - \lvert E_{F\text{-}U_2}\rvert$ | 0.36 | 1.68 |
| $\lvert E_{AF\text{-}U_3}\rvert - \lvert E_{F\text{-}U_3}\rvert$ | 0.42 | 1.73 |
| $\lvert E_{AF\text{-}U_4}\rvert - \lvert E_{F\text{-}U_4}\rvert$ | 0.34 | 0.20 |

electronic structure calculations of the non-molecular stoichiometric compounds $Sr_2CoO_2Cu_2S_2$ and $Ba_2CoO_2Cu_2S_2$ were carried out using VASP [117, 118]. Electron correlation plays a predominant role when magnetic interactions in transition metal-containing materials are studied. Indeed, the strongly correlated character of the electrons in the open-shell 3d levels of $Co^{2+}$ should be described accurately, and the self-interaction error related to the density functional description of the magnetic unpaired Co-3d electrons should be corrected. In this context, the Hubbard correction to the KSDFT has been considered employing the Dudarev approach [119, 120]. In the latter formalism, the term $U_{eff} = U - J$ representing difference between the on-site (U) and inter-site (J) interactions is added as a penalty-functional to the KSDFT Hamiltonian. Thus, J was kept fixed at 0 eV, whereas different values were tested for the U parameter. All results were obtained using the refined experimental magnetic structures [121] and

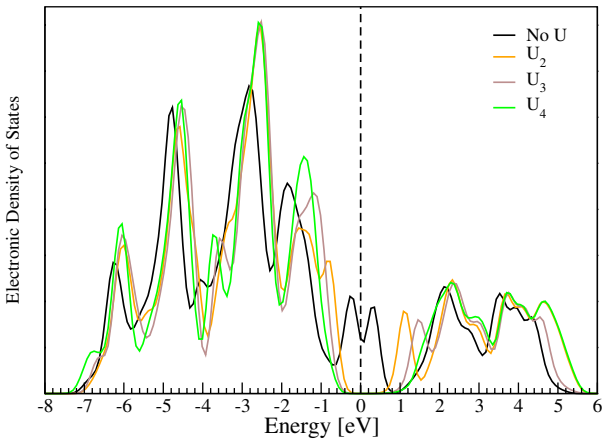


**Figure 9.** The effect of inclusion of the on-site electron-electron repulsion parameter U on the electronic density of states for $Sr_2CoO_2Cu_2S_2$ ($U_n$ means $U = n$ eV). With increasing $n$, the insulating behavior is well recovered through the opening of the band-gap.

adopting a fixed spin configuration corresponding to that observed. Further, non-collinear magnetic calculations considering the additional spin-orbit Hamiltonian were performed. The effect of spin-orbit coupling (SOC) was investigated adopting different easy-axis orientations (in-plane and axial) to evaluate the dependence of the orbital magnetic moment contribution and the magnetic anisotropy. Table 4 gathers the calculated stabilization energies of the observed AF phase over an alternative ferromagnetic state. Also given is the non-magnetic case to show the effect of the spin polarization. If the on-site correction through the U parameter was not included in the calculations (i.e. U = 0 eV) spin polarization would lead to a stable state (either AF or F) over the non-magnetic case. Furthermore, the ferromagnetic state was favored over the AF state by 0.53 eV for $Sr_2CoO_2Cu_2S_2$ and 0.74 eV for $Ba_2CoO_2Cu_2S_2$. The inclusion of the U parameter is found to stabilize strongly the observed AF ground state over the ferromagnetic one for both compounds, by 0.42 eV in $Sr_2CoO_2Cu_2S_2$ and 1.73 eV in $Ba_2CoO_2Cu_2S_2$, for an optimal on-site correction of 3 eV ($U_3$). Figure 9 shows the total electronic density of states (EDOS) for $Sr_2CoO_2Cu_2S_2$. As expected for "standard" DFT-based methods, without explicit treatment of the strong electron correlation, the insulating character predicted for this type of materials is not reproduced. Instead a metallic-like character is obtained. This is corrected by adding the on-site interaction. Therefore, there is an opening of the band-gap at the Fermi level ($E_F$) as U is increased, leading hence to the expected insulating characted of this material. Similarly the same behavior is reproduced for $Ba_2CoO_2Cu_2S_2$. Considering the optimal value $U_3$, the total EDOS for the two compounds are reported in Figure 10.

The site-projected EDOS for $Sr_2CoO_2Cu_2S_2$ is shown in Figure 11. Clearly the top of the valence band is composed of well-mixed Co-3d/O-2p states and Cu-3d/S-3p states. So the changes in Cu-S, Co-O and Co-S bond lengths when $Sr_2CoO_2Cu_2S_2$ is subject to mild oxidation result from oxidation both of the Cu-3d/S-3p states and the mainly Co-3d states. The suggestion in ref. [122] that there is a temperature dependent electron transfer between the $CoO_2$ and $Cu_2S_2$ layers is also certainly not implausible from our calculations [121] although it is not clear whether the sample in ref. [122] is stoichiometric or slightly copper deficient as a result of air exposure. Figure 12 compares the angular-momentun EDOS for $Sr_2CoO_2Cu_2S_2$ and $Ba_2CoO_2Cu_2S_2$. These results show that the effect of increasing the axial distention of the $CoO_4S_2$ octahedron is profound. In $Sr_2CoO_2Cu_2S_2$ the result is that the spin-up contribution of the EDOS lies below $E_F$ while the down components of the $d_{z^2}$, $dd_{xy}$, and $d_{x^2-y^2}$ are unoccupied (above $E_F$). This situation corresponds to the configuration derived above and shown in Figure 13(b) & (c). In the case of $Ba_2CoO_2Cu_2S_2$ the calculations show a slightly

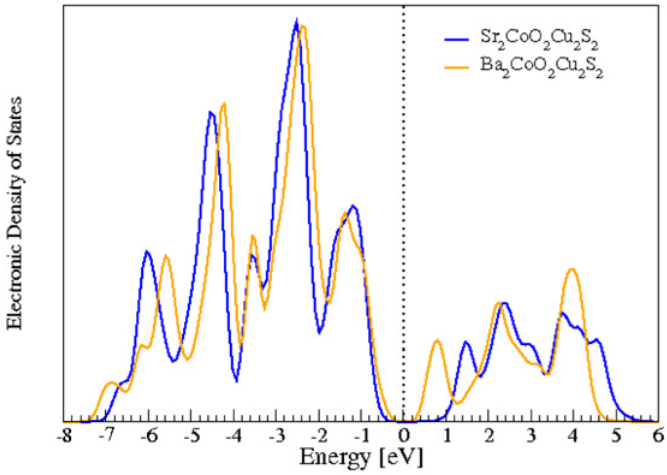


**Figure 10.** Total electronic density of states for $Sr_2CoO_2Cu_2S_2$ and $Ba_2CoO_2Cu_2S_2$ for U = 3 eV [121].

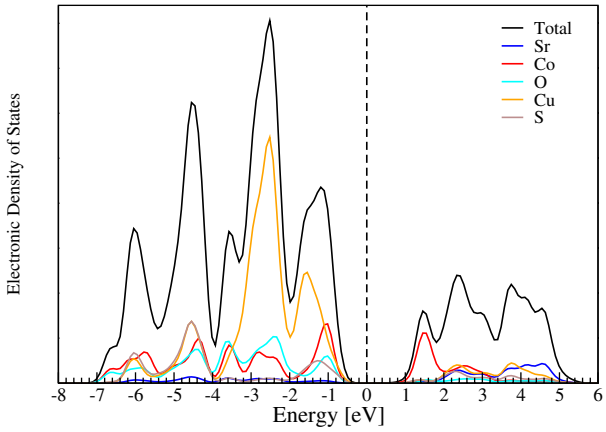


**Figure 11.** Total and site projected EDOS for $Sr_2CoO_2Cu_2S_2$ obtained for the AF state for U = 3 eV [121].

different picture (Figure 12). With the increased axial distention of the $CoO_4S_2$ octahedron, the picture that emerges from the calculations is that now the $d_{z^2}$ spin-down component is occupied while the $d_{xz}$ and $d_{yz}$ down component is only half occupied. There is also greatly increased mixing of the $d_{z^2}$ and $d_{xz}$, $d_{yz}$ spin orbitals compared with the $Sr_2CoO_2Cu_2S_2$ case.

The calculations suggest that in our simple ligand field picture the $Ba_2CoO_2Cu_2S_2$ system is very close to the crossover from the $4A_{2g}$ (Figure 13 case(c)) to $4E_g$ (Figure 13 case(d)) and the $d_{z^2}$ is very close to degenerate with $d_{xy}$ and $d_{xz}$. Spin orbit coupling (SOC) mixes $d_{z^2}$ with $d_{xz,yz}$ to an extent which depends on the energy separation of the levels and since the orbitals are close to degenerate in energy we propose that this is the origin of the very large orbital contribution to the moment in $Ba_2CoO_2Cu_2S_2$. It is unclear whether the ground term in this case is $4E_g$ (corresponding to the configuration $(d_{z^2})^2(d_{xz}, d_{yz})^3(d_{xy})^1(d_{x^2-y^2})^1$ with a first order orbital moment or whether the ground term is $4A_{2g}$ (corresponding to the configuration $(d_{xz}, d_{yz})^4(d_{z^2})^1(d_{xy})^1(d_{x^2-y^2})^1$ with the $4E_g$ close in energy. From our calculations (Figure 12), in $Sr_2CoO_2Cu_2S_2$ the anisotropy is smaller which would place $d_{z^2}$ above $d_{xz,yz}$ by about 2000 $cm^{-1}$ (0.25 eV) and roughly degenerate with $d_{xy}$ (i.e. case (c) in Figure 13). The many electron SOC parameter, $\lambda$, for $Co^{2+}$ is around $-200\,cm^{-1}$ ($-25$ meV) so the

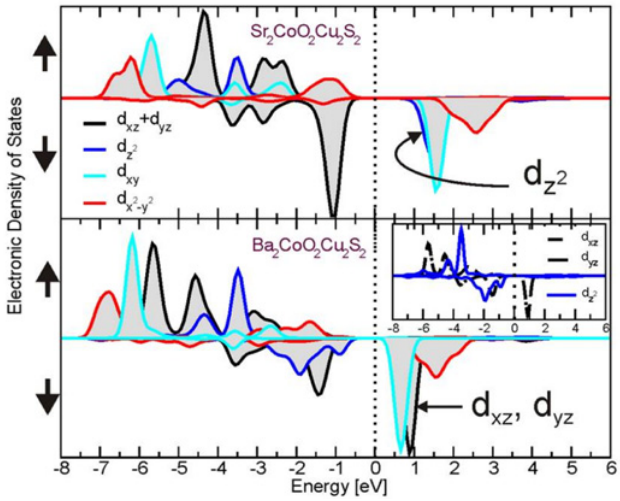


**Figure 12.** Angular-momentun resolved EDOS for the Co-3d levels (l = 2) for $Sr_2CoO_2Cu_2S_2$ (upper panel) and $Ba_2CoO_2Cu_2S_2$ (lower panel) [121].

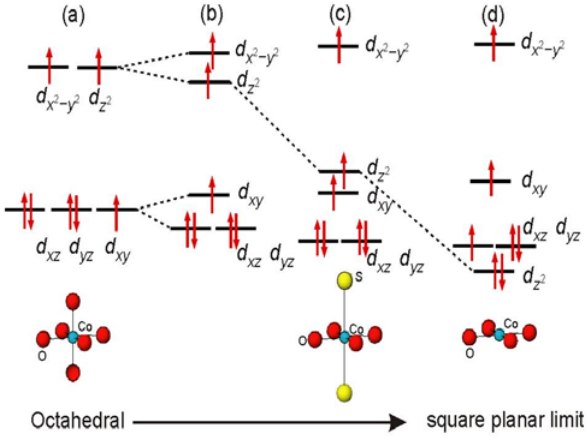


**Figure 13.** Cartoon showing the d orbital splitting for molecular high spin $Co^{2+}$ systems ranging from purely octahedral (a) to purely square planar (d) via a slightly distended octahedron (b) and the highly anisotropic arrangement appropriate to $Sr_2CoO_2Cu_2S_2$ (c). The $d_{x^2-y^2}$ and $d_z^2$ orbitals are $\sigma$-antibonding and the $d_{xy}$, $d_{xz}$ and $d_{yz}$ are $\pi$-antibonding.

mixing of the orbitals in $Sr_2CoO_2Cu_2S_2$ will be significantly less than in the case of $Ba_2CoO_2Cu_2S_2$ and the orbital moment will be correspondingly reduced. Finally, delocalization onto the ligands tends to reduce the spin and orbital moments [123]. As the Co-O distance increases this reduction is expected to decrease further enhancing the ordered moment and this may partially account for the larger ordered moment in $Ba_2CoO_2Cu_2S_2$.

Calculations were also performed in which SOC was included (Table 5). These revealed two points: firstly there is a strong in-plane magnetic anisotropy in these systems consistent with the experimental observation that the magnetic moments have their major component oriented in the $CoO_2$ planes. Secondly the calculations showed qualitatively that the orbital component of the magnetic moment should be larger in the case of $Ba_2CoO_2Cu_2S_2$ than $Sr_2CoO_2Cu_2S_2$, although the difference in the size

**Table 5.** Results of the non-collinear calculations with spin orbit coupling included.

| Compound | In-plane magnetic anisotropy $\Delta E_{\parallel-\perp}$ (meV) | In-plane orbital moment ($\mu_B$) | Out-of-plane orbital moment ($\mu_B$) |
|---|---|---|---|
| $SrCoO_2Cu_2S_2$ | 30 | 0.3 | 0.06 |
| $BaCoO_2Cu_2S_2$ | 30 | 0.4 | 0.2 |

of the experimental moments of about $0.7\mu_B$ is about a factor of 5 larger than that suggested by the calculations [121] as is commonly found in comparable computations due to the nature of the numerical integration in these calculations [124]. The calculations predict a larger $z$ component of the magnetic moment in $Ba_2CoO_2Cu_2S_2$ than in $Sr_2CoO_2Cu_2S_2$ in agreement with the measurements [121]. The large orbital moments in these systems apparently result from spin-orbit mixing of the unequally populated $d_{xz}$, $d_{yz}$ and $d_z^2$ orbitals which are reckoned to be almost degenerate when the environment of $Co^{2+}$ is very square planar. Thus the experimental observations of the AF ground states and the changes in properties resulting from replacement of Sr by Ba are well supported by the ab initio calculations.

## 6. MAGNETIC LATTICE DYNAMICS

In the previous sections we have introduced three applications of DFT to magnetic structure problems studied by neutron diffraction. Therein a direct estimate of the relevant magnetic aspects has been performed. Unexpectedly, magnetism can manifest itself implicitly in some complex cases exhibiting remarkable properties or are the subject of critical phenomena, like high temperature superconductivity (HTSC). Therefore, in this example we are interested in phonons (quantum of vibrations) in the recently discovered FeAs layered pnictides. Studying phonons may help to clarify the mechanism of Cooper pair formation (zero resistivity) in HTSC. Four types of parent FeAs-based superconductors have mainly been discovered: RFeAsO [125] (R: Rare earth elements) or AFeAsF (A: alkaline-earth elements), $AFe_2As_2$ [126–128], and LiFeAs [129]. In the following, the 122 ($AFe_2As_2$; A = {Ca, Sr, Ba}) and 1111 (AFeAsF; A = {Ca, Sr}) case studies are shown. Figure 14 shows a schematic illustration of their crystal structure in the room temperature (RT), tetragonal, paramagnetic phase [126, 127, 134] and in the low temperature (LT) orthorhombic phase.

Structural, electronic and magnetic properties of these compounds are remarkably similar. The parent FeAs pnictides show a well pronounced spin density wave through transitions from the paramagnetic, tetragonal phase to an antiferromagnetically (AF) ordered, orthorhombic phase [126, 127, 134, 135]. Consequently, magnetism couples to the structure in these systems. Figure 15 shows schematically the experimentally refined orientations of the Fe moments [126]. The moments are oriented ferromagnetically parallel to the y-axis, and adopt an antiferromagnetic alignment along the x- and $z$-axes.

In $AFe_2As_2$ (A = Ba, Ca and Sr) electron/hole doping or pressure suppresses these phase transitions and the related magnetic ordering and induces superconductivity through electron pairing at low temperatures, supporting the idea of a possible coupling between spin degrees of freedom and superconductivity in the iron pnictides. Raman scattering measurements of the temperature dependence of zone center phonons modes in $Ba_{1-x}K_xFe_2As_2$ [136] and $Ba(Fe_{1-x}Co_x)_2As_2$ shows renormalization of the active phonons on cooling through the tetragonal-to-orthorhombic transition temperature where the magnetic ordering occurs, providing a signature of spin-phonon coupling [137].

On the computational side, magnetism has been found to be of considerable importance to treat reasonably the oxygen-based and oxygen-free iron-pnictides. In a very short time, a huge amount of work has been done to highlight the discrepancies between non-magnetic and magnetic calculations to describe the Fe-pnictides (Refs. [138–145] and references therein). Ab-initio calculations for $BaFe_2As_2$ show evidence for a selective coupling of electronic and spin degrees of freedom with phonons [145].

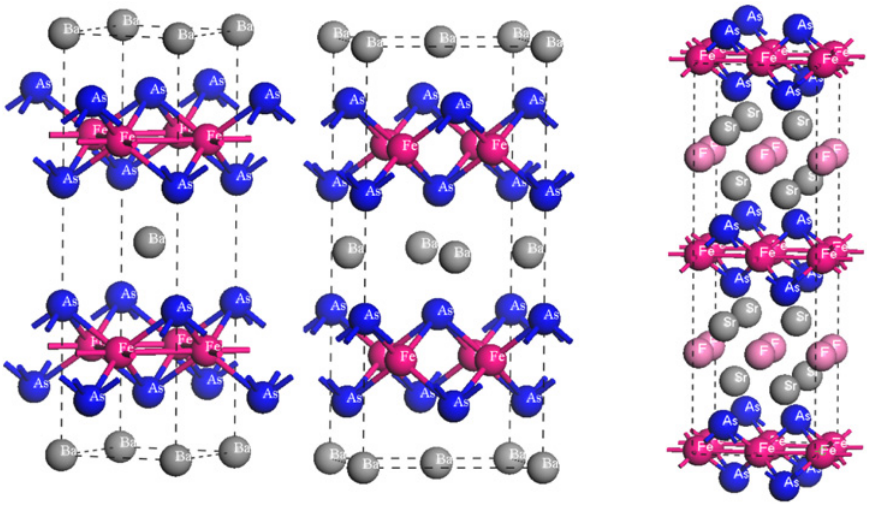

**Figure 14.** Schematic illustration of the crystal structure of the 122 ($MFe_2As_2$; M = {Ca, Sr, Ba} – Left: high temperature tetragonal structure, middle: low temperature orthorhombic structure) and the 1111 (MFeAsF; M = {Ca, Sr} – Right panel) oxygen-free FeAs pnictides [145–147].

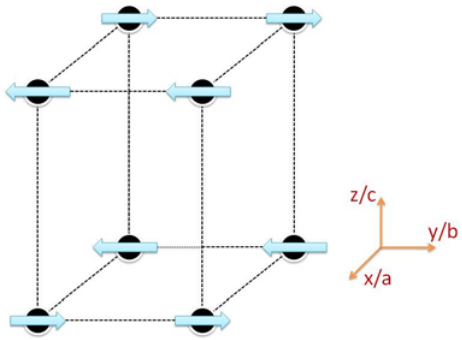


**Figure 15.** Schematic illustration of the spin ordering of the Fe magnetic sites in the low-temperature orthorhombic phase [126, 127].

Furthermore, the measurement of the phonon density of states for Ca 1111 $CaFe_{1-x}Co_xAsF$ ($x = 0$, 0.06, 0.12) indicates [147] that stronger spin-phonon interactions play an important role for the emergence of superconductivity in these compounds. It is of a primary interest to investigate the direct effect of the spin degrees of freedom on the phonon dynamics in the parent compounds in the LT phase where the spin density wave occurs. In this context we consider magnetic ordering (Figure 15), observed in the orthorhombic phase (Fmmm (69) [$D_{23}^{2h}$] and Cmma (67) [$D_{21}^{2h}$] for the 122 and 1111 families, respectively) and we aimed at probing the spin-phonon coupling. Non magnetic calculations (NM) are used as a reference and compared to the magnetic case (MAG) where the additional spin degree of freedom are explicitly included.

Ab-initio calculations were performed using the VASP package [117, 118]. NM calculations consist of neglecting the spin polarization while calculating the inter-atomic force constants of the dynamical matrix. In the MAG calculations, the spin degrees of freedom are included when calculating the inter-atomic force constants. It is worthwhile to note that although the crystallographic

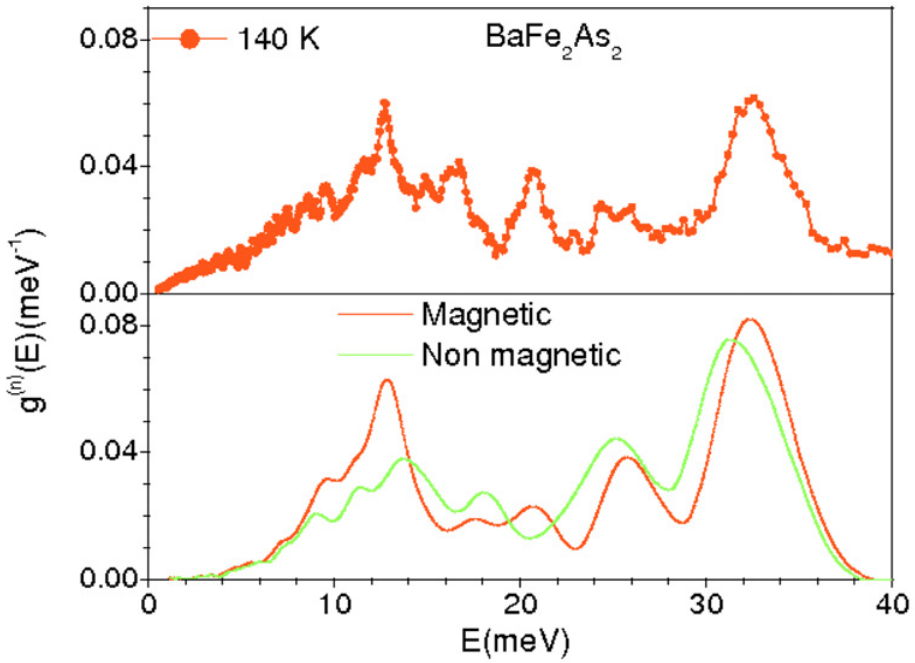


**Figure 16.** Comparison between the experimental and calculated phonon spectra for $BaFe_2As_2$. The calculated spectra have been convoluted with a Gaussian of FWHM of 10% of the energy transfer in order to describe the effect of energy resolution in the experiment. All the phonon spectra are normalized to unity. The experimental phonon data for $BaFe_2As_2$ are taken from Ref. [145].

properties in the Fe-pnictides are better described considering the magnetic interactions, the calculated magnetic moments are overestimated compared to the measurements from neutron scattering and $\mu$SR experiments. Different explanations were proposed ranging from frustration and (a non-observed) lattice distortion to spin fluctuations and effect of lattice-dimensionality (Refs. [126, 145, 148–152] and references therein provide some relevant details in this regard for both measured and calculated magnetic moments in the Fe-pnictides). In the lattice dynamics calculations, in order to determine all inter-atomic force constants, the super cell approach has been adopted [153, 154]. Total energies and inter-atomic forces were calculated for the structures resulting from individual displacements of the three symmetry inequivalent atoms along the three Cartesian directions ($\pm x$, $\pm y$ and $\pm z$). Phonon spectra and properties were extracted in subsequent calculations using the Phonon software [154]. The detailed procedure is explained in a general way in Ref. [5], and more precisely for the present case in Refs. [145–147]. The comparison between the experimental phonon spectra and ab-initio calculations for $BaFe_2As_2$ is shown in Figure 16. The NM calculations do not describe accurately the measured phonon spectrum. There is a pseudo gap at the 21 meV peak position and frequencies of the stretching modes are underestimated. Interestingly, MAG calculations recover all the observed features, especially the peak at 21 meV. An improvement is also observed for the Fe-As stretching modes. This is a clear signature of a magneto-structural correlation which affects phonon dynamics, and could indicate a selective spin-phonon coupling as recently suggested [145]. The situation is similar in the $CaFe_2As_2$ and $SrFe_2As_2$ cases shown in Figure 17, where magnetism improves the agreement [146]. It is also worthwhile highlighting the importance of the peak at 21 meV in $BaFe_2As_2$. Experimentally it corresponds to an axially (z) polarized $A_{1g}$ mode of the As atoms. It has been shown that a small displacement of the As along the z-axis has a significant impact on the electronic and magnetic features of the $BaFe_2As_2$ [149, 151, 152]. This is clearly evident in the lattice dynamical calculations.

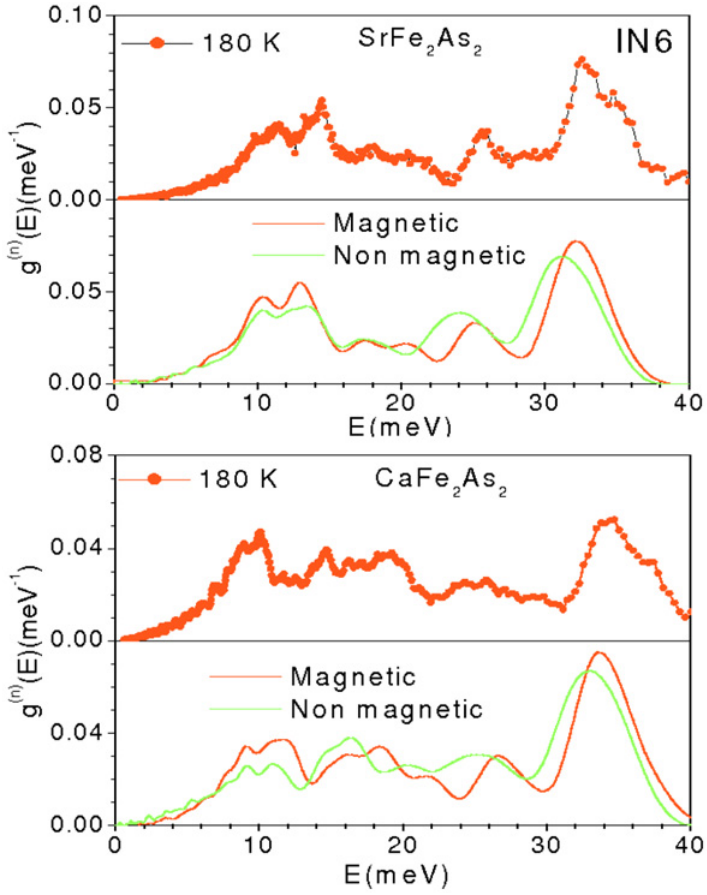


**Figure 17.** Comparison between the experimental and calculated phonon spectra for $AFe_2As_2$ (A = Sr, Ca). The calculated spectra have been convoluted with a Gaussian of FWHM of 10% of the energy transfer in order to describe the effect of energy resolution in the experiment. The experimental phonon data for $CaFe_2As_2$ are taken from Ref. [146]. All the phonon spectra are normalized to unity.

Now we analyze the 1111 case by comparing the two systems CaFeAsF and SrFeAsF. Figure18 compares their respective measured and calculated phonon spectra. The observed features in the experimental data are well reproduced computationally when magnetism is considered, as is the case for the 122 compounds. Both the peak positions and intensities are significantly improved, especially for the low-frequency and mid-frequency ranges. In SrFeAsF, the modes within the range 20–28 meV involving Fe and As are well resolved and match better the observations when magnetic interactions are included. Similarly, the low-lying 0 -12 meV frequency range is well described in CaFeAsF through a correct $E^2$-dependence in the MAG calculations. This is also the case for the intensity profile in 20–30 meV. Furthermore for both systems, the stretching modes due to F (shoulder around 45 meV) are found in the correct frequency position, indicating a good description of both structural and chemical interactions involving the lightest element F.

For all the compounds (122 and 1111), the importance of the magnetic interactions to describe accurately the inter-atomic force constants was clearly demonstrated. As revealed by spin-polarized DFT calculations, the observed magnetic interactions must be included in the lattice dynamical calculations to describe accurately the phonons in the FeAs pnictides.

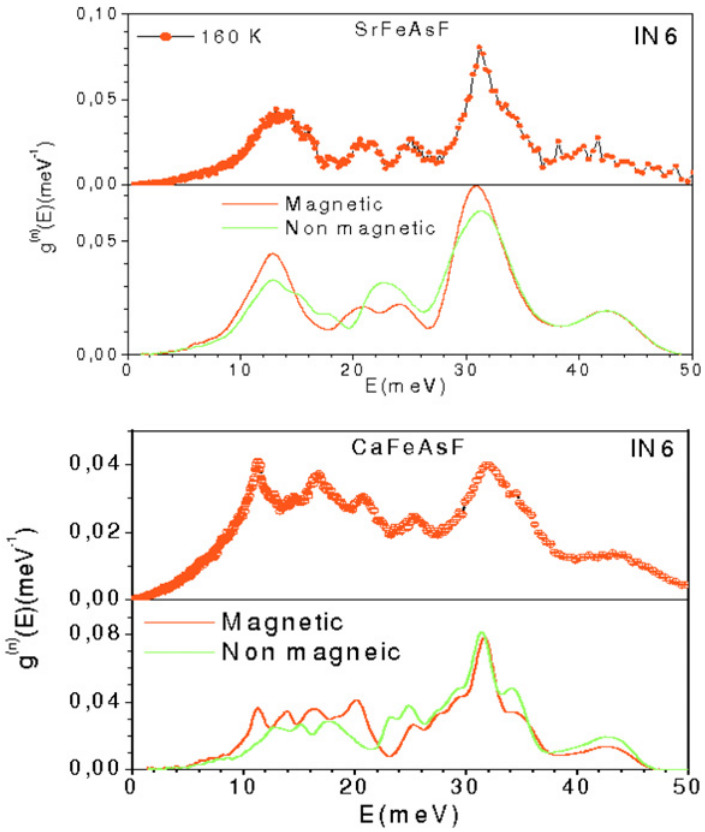


**Figure 18.** Comparison of the experimental phonon spectra for SrFeAsF and CaFeAsF. The phonon spectra are measured with an incident neutron wavelength of 5.12 Å using the IN6 spectrometer at the ILL. The experimental phonon data for CaFeAsF are taken from Ref. [147]. All the phonon spectra are normalized to unity.

## 7. CONCLUSIONS

We have introduced density functional theory and highlighted some successful attempts to improve it for magnetism including further effects like spin polarization and strong electron correlation. Some selected examples were presented to demonstrate the robustness of the DFT methods to treat complex materials with intriguing magnetic properties. The examples have used the simplest, collinear representation of magnetic order, extending up to including spin-orbit coupling to describe large magnetic moments and magnetic anisotropy, and Hubbard corrections and hybrid functionals to describe electron correlation. Neutron scattering measurements, and other scattering techniques where magnetism is directly or indirectly concerned, can greatly benefit from approaching the results of observations (elastic and inelastic processes) with DFT simulations.

## References

[1] Materials with Complex Behaviour: Modelling, Simulation, Testing, and Applications by Andreas Öchsner, Lucas Filipe Martins da Silva, Holm Altenbach (2010) Springer Publisher.

[2] M. Calin, J. Das, K.B. Kim, S. Pauly, N. Mattern, J. Eckert, Mater. Science Forum 633 (2010) 665.

[3] F. Boerrnert, C. Boerrnert, S. Gorantla, X. Liu, A. Bachmatiuk et al., Phys. Rev. B. 81 (2010) 85439.
[4] Essentials of Computational Chemistry: Theories and Models by C. J. Cramer, 2nd ed. (2004) John Wiley & Sons Inc.
[5] M. Johnson et al., JDN 16 - Collection SFN 10 (2010) 427.
[6] Modern Magnetic Materials: Principles and Applications by Robert C. O'Handley (2000) John Wiley & Sons Inc.
[7] Neutron Scattering from Magnetic Materials, Edited by T. Chatterji (2006) Elsevier B. V.
[8] DFT Studies of Magnetic Semiconductors and Multiferroics: Density Functional Applications, By Adrian Ciucivara (2009) VDM Verlag Publisher.
[9] M. Moshinsky, Group Theory and the Many-Body Problem (Gordon and Breach 1968)
[10] D. R. Hartree, Proc. Cambridge. Phil. Soc. 24 (1928) 89, III.
[11] P. Atkins, Molecular Quantum Mechanics. Oxford University Press (1983).
[12] P. Davies, Quantum Mechanics. Chapman and Hall (1994).
[13] W. Greiner, J. Reinhardt, Quantum Electrodynamics, 2nd ed. (Springer-Verlag, Berlin, Heidelberg 1994).
[14] J. C. Slater, Phys. Rev. 35 (1930) 250.
[15] V. Fock, Z. Physik. 61 (1930) 126.
[16] J. Tobochnik, H. Gould, and K. Mulder, Comp. Phys. 4(4) (1990) 431.
[17] G. D. Purvis and Y. Öhrn, J. Chem. Phys. 60 (1974) 4063.
[18] U. Schollwöck, Rev. Mod. Phys. 77 (2005) 259.
[19] H. Thomas, Proc. Camb. Phil. Soc. 23 (1927) 542.
[20] E. Fermi, Rend. Accad. Lincei, 6 (1927) 602.
[21] E. Fermi, Z. Phys. 48 (1928) 73.
[22] E. Fermi, Rend. Accad. Lincei, 7 (1928) 342.
[23] P. A. M. Dirac, Proc. Camb. Phil. Soc. 26 (1930) 376.
[24] C. F. von Weizsäcker, Z. Phys. 96 (1935) 431.
[25] E. Teller, Rev. Mod. Phys. 34 (1962) 627.
[26] W. Yang, Phys. Rev. A 34 (1986) 4575.
[27] J. C. Slater, Phys. Rev. 81 (1951) 385.
[28] J. C. Slater, Adv. Quantum Chem. 6(1964) 1.
[29] J. C. Slater, K. H. Johnson, Phys. Rev. 135 (1972) 544.
[30] P. Hohenberg, W. Kohn, Phys. Rev. B 136 (1964) 864.
[31] H. English, R. English, Physica, 121A (1983) 253.
[32] E. H. Lieb, Int. J. Quant. Chem., XXIV (1983) 243.
[33] W. Kohn, L. J. Sham, Phys. Rev. 140 (1965) A1133.
[34] F. M. Bickelhaupt, E. J. Baerends, Reviews in Computational Chemistry 15 (2000) 1.
[35] P. Geerlings, F. De Proft, W. Langenaeker, Chem. Rev 103(5) (2003) 1795.
[36] R. G. Pearson, Chemical Hardness, Wiley-VCH (1997).
[37] D. M. Ceperley, B. J. Alder, Phys. Rev. Lett. 45 (1980) 566.
[38] S. J. Vosko, L. Wilk, M. Nusair, Can. J. Phys. 58 (1980) 1200.
[39] D. Pines, Elementary Exitations in Solids. Benjamin (1963).
[40] U. von Barth, L. Hedin, J. Phys. C. 5 (1972) 1629.
[41] M. M. Pant, A. K. Rajagopal, Solid State Commun., 5 (1972) 1157.
[42] O. Gunnarson and B. I. Lundqvist, Phys. Rev. B, 13 (1976) 4274.
[43] J. P. Perdew, Phys. Rev. Lett. 55 (1985) 1665.
[44] A. D. Becke, J. Chem. Phys. 84(8) (1986) 4524.
[45] A. D. Becke, J. Chem. Phys. 96(3) (1992) 2155.
[46] A. D. Becke, J. Chem. Phys. 97(12) (1992) 9173.
[47] A. D. Becke. J. Chem. Phys. 107(20) (1997) 8554.

[48] J. P. Perdew, Y. Wang, Phys. Rev. B, 33(12) (1986) 8800.
[49] J. P. Perdew, Phys. Rev. B, 33(12) (1986) 8822.
[50] Y. Wang and J. P. Perdew, Phys. Rev. B, 43(11) (1991) 8911.
[51] J. P. Perdew and Y. Wang, Phys. Rev. B, 45(23) (1992) 13244.
[52] A. Schindlmayr, T. J. Pollehn and R.W. Godby, Phys. Rev. B 58 (1998)12684.
[53] A. D. Becke, Phys. Rev. A, 38 (1988) 3098.
[54] J. P. Perdew, K. Burke, M. Ernzerhof, Phys. Rev. Lett. 77 (1996) 3865; 78 (1997) 1396(Erratum).
[55] C. Lee, W. Yang, R. G. Parr, Phys. Rev. B 37 (1988) 785.
[56] R. Colle, O. Salvetti, Theor. Chim. Acta 37 (1975) 329.
[57] B. Miehlich, A. Savin, H. Stoll, H. Preuss, Chem. Phys. Lett. 157 (1989) 200.
[58] J. P. Perdew, K. Schmidt, in Density Functional Theory and Its Application to Materials, edited by V. van Doren, C. Van Alsoney, and P. Geerlings (AIP, Melville, New York, 2001).
[59] A. E. Mattson, Science 298 (2002) 759.
[60] J. Harris, Phys. Rev. B. 29 (1984) 1648.x
[61] A. D. Becke, J. Chem. Phys. 88 (1988) 1053.
[62] A. D. Becke, J. Chem. Phys. 98 (1993) 1372.
[63] A. D. Becke, J. Chem. Phys. 98 (1993) 5648.
[64] P. Perdew, in Electronic Structure of Solids, edited by P. Ziesche and H. Eachrig (Akademie Verlag, Berlin, 1991).
[65] J. P. Perdew, J. A. Che- vary, S. H. Vosko, K. A. Jackson, M. R. Pederson, D. J. Singh, C. Fiolhais, Phys. Rev. B 46 (1992) 6671.
[66] J. P. Perdew, Y. Wang (unpublished).
[67] P. J. Stephens, F. J. Devlin, C. F. Chabalowski, M. J. Frisch, J. Phys. Chem 98 (1994) 11623.
[68] A. D. Becke, J. Chem. Phys 104 (1996) 1040.
[69] J. P. Perdew, M. Ernzerhof, A. D. Burke, J. chem. Phys 105 (1996) 9982.
[70] A. D. Burke, M. Ernzerhof, J. P. Perdew, Chem. Phys. Lett 265 (1997) 115.
[71] Zbiri et al., Theor. Chem. Acc.,, 125 (2010) 445.
[72] J. A. Pople, M. Head-Gordon, D. J. Fox, K. Raghavachari, L. A. Curtiss, J. Chem. Phys. 90 (1989) 5622.
[73] J. D. Morrison, R. E. Moss Mol. Phys 41 (1980) 491.
[74] R. E. Moss Mol. Phys 53 (1984) 269.
[75] L. L. Foldy, S. A. Wouthuysen Phys. Rev 78 (1950) 29.
[76] W. Pauli, Z. Phys 43 (1927) 601.
[77] E. van Lenthe, P. E. S. Wormer, A. van der Avoird J. Chem. Phys 107 (1997) 2488.
[78] M. Filatov, Chem. Phys. Lett 365 (2002) 222.
[79] W. G. Richards, H. P. Trivedi, D. L. Cooper, Spin-Orbit Coupling in Molecules, Clarendon Press, Oxford Science Publications, 1981.
[80] G. te Velde, F. M. Bickelhaupt, E. J. Baerends, C. F. Guerra, S. J. A. van Gisbergen, J. G. snijders, T. Ziegler J. Comp. Chem 22 (2001) 931.
[81] Gaussian 03, Revision C.02, M. J. Frisch et al., Gaussian, Inc., Wallingford CT, 2004.
[82] Molecular Magnetism, By O. Kahn (1993) Wiley-VCH Inc.
[83] Goodenough, J B and Zhou, J-S, Structure and Bonding 98 (2001) 17.
[84] Magnetism and the Chemical Bond, By Goodenough, J B (1963) Interscience-Wiley, New York.
[85] Kanamori J., J. Appl. Phys. Suppl. 31 (1960) 145.
[86] Zbiri et al., Inorg. Chim. Acta., 359 (2006) 1193.
[87] P.A.M. Dirac, Proc. Roy. Soc. London 112 (1926) 661.
[88] P.A.M. Dirac, Proc. Roy. Soc. London 123 (1929) 714.
[89] W. Heisenberg, Z. Phys. 38 (1926) 411.
[90] W. Heisenberg, Z. Phys. 49 (1928) 619.

[91] J.H. Van Vleck, Theory of Electric and Magnetic Susceptibilities, Oxford University Press, London, 1932.
[92] L.J. Noodleman, Chem. Phys. 74 (1981) 5737.
[93] L.J. Noodleman, E.R. Davidson, Chem. Phys. 109 (1986) 131.
[94] L.J. Noodleman, C.Y. Peng, D.A. Case, J.M. Mouesca, Coord.Chem. Rev. 144 (1995) 199.
[95] O. Kahn, S. Sikorov, J. Gouteron, S. Jeannin, Y. Jeannin, Inorg. Chem. 22 (1983) 2877.
[96] E. Ruiz, J. Cano, S. Alvarez, P.J. Alemany, J. Am. Chem. Soc. 120 (1998) 11122.
[97] E. Ruiz, J. Cano, S. Alvarez, P. Alemany, Int. J. Quantum Chem. 20 (1999) 1391.
[98] A. Bencini, F. Totti, Int. J. Quantum Chem. 101 (2005) 819.
[99] E. Ruiz, P. Alemany, S. Alvarez, J. Cano, J. Am. Chem. Soc. 119 (1997) 1303.
[100] F. Fabrizi de Biani, E. Ruiz, J. Cano, J.J. Novoa, S. Alvarez, Inorg.Chem. 39 (2000) 3221.
[101] E. Sola, F. Torres, M.V. Jimmenez, J.A. Lopez, S.E. Ruiz, F.J.Lahoz, A. Elduque, L.A. Oro, J. Am. Chem. Soc. 123 (2001) 11925.
[102] W. Plass, Magnetic Interactions in Metal Clusters, John von Neumann for Computing, Julich, 2003.
[103] J.P. Perdew, M. Ernzerhof, K. Burke, A. Savin, Int. J. Quantum Chem. 61 (1997) 197.
[104] L.J. Noodleman, D.A. Case, Inorg. Chem. 38 (1992) 423.
[105] E. Goldstein, B. Beno, K.N. Houk, J. Am. Chem. Soc. 118 (1996) 6036.
[106] M. Nishino, S. Yamanaka, Y. Yoshioka, K.J. Yamagushi, J. Phys. Chem. A 101 (1997) 705.
[107] A. Szabo, N.S. Ostlund, Modern Quantum Chemistry, McGraw-Hill, 1989.
[108] E. Ruiz, C. de Graaf, P. Alemany, S. Alvarez, J. Phys. Chem. A 106 (2002) 4938.
[109] M.A. Aebersold, B. Gillon, O. Plantevin, L. Pardi, O. Kahn, P. von Bergerat, I. Seggern, F. Tuczek, L. Öhrström, A. Grand, E.Lelièvre-Berna, J. Am. Chem. Soc. 120 (1998) 5238.
[110] H. Fuess et al., Acta Crystallogr.,Sect. B: Struct. Crystallogr. Cryst. Chem. 26 (1970) 2036.
[111] E. E. Sauerbrei et al., Acta Crystallogr.,Sect. B: Struct. Crystallogr. Cryst. Chem. 29 (1973) 2034.
[112] Y. Chen et al., Phys. Rev. B 74 (2006) 014430.
[113] N. R. Wilson, O. A. Petrenko, and G. Balakrishnan, J. Phys.: Condens. Matter 19 (2007) 145257.
[114] N. Qureshi, M. Zbiri et al., Phys. Rev. B, 79 (2009) 094417.
[115] Schmidt et al., J. Comput. Chem. 14 (1993) 1347.
[116] M. S. Gordon, M. A. Freitag, P. Bandyopadhyay, J. H. Jensen, V.Kairys, and W. J. Stevens, J. Phys. Chem. A 105 (2001) 293.
[117] Kresse and J. Furthmüller, Comput. Mater. Sci. 6 (1996) 15.
[118] Kresse and D. Joubert, Phys. Rev. B 59 (1999) 1758.
[119] Dudarev et al., Phys. Rev. B 57 (1998) 1505
[120] Anisimov et al., Phys. Rev. B 44 (1991) 943.
[121] C. F. Smura, D. R. Parker, M. Zbiri, M. R. Johnson, Z. A. Gál and S. J. Clarke, *J. Am. Chem. Soc* **133** (2011) 2691.
[122] S. Okada et al., Applied Physics, 95 (2004) 6816.
[123] J. Hubbard and W. Marshall, Proc. Phys. Soc. (London) 86 (1965) 561.
[124] H. J. Xiang et al., Phys. Rev. Lett. 100 (2008) 167207.
[125] Kamihara Y, Watanabe T, Hirano M and Hosono H 2008 *J. Am. Chem. Soc.* **130** 3296
[126] Rotter M, Tegel M, Johrendt D, Schellenberg I, Hermes W and Pöttgen R 2008 *Phys. Rev.* B **78** 020503
[127] Rotter M, Tegel M and Johrendt D 2008 *Phys. Rev. Lett.* **101** 107006
[128] Pöttgen R and Johrendt D 2008 *Z. Naturforsch.* B **63b** 1135
[129] Wang X C, Liu Q Q, Lv Y X, Gao W B, Yang L X, Yu R C, Li F Y and Jin C Q 2008 *Solid State Communications.* **148** 538
[130] Wu G, Xie Y L, Chen H, Zhong M, Liu R H, Shi B C, Li Q J, Wang X F, Wu T, Yan Y J, Ying J J and Chen X H 2009 *J. Phys. Cond. Matt* **21** 142203

[131] Cheng P, Shen B, Mu G, Zhu X, Han F, Zeng B and Wen H H 2009 *Europhys. Lett* **85** 67003
[132] Ren Z A et al., 2008 *Chin. Phys. Lett.* **25** 2215
[133] Wang C, Li L, Chi S, Zhu Z, Ren Z, Li Y, Wang Y, Lin X, Luo Y, Jiang S, Xu X, Cao G and Xu Z 2008 *Europhys. Lett* **83** 67006
[134] Su Y, Link P, Schneidewind A, Wolf T, Adelmann P, Xiao Y, Meven M, Mittal R, Rotter M, Johrendt D, Brueckel T and Loewenhaupt M 2009 *Phys. Rev.* B **79** 064504
[135] Xiao Y, Su Y, Mittal R, Chatterji T, Hansen T, Kumar C M N, Matsuishi S, Hosono H and Brueckel T 2009 *Phys. Rev.* B **79** 060504
[136] Sun M R G L, Sun D L, Lin C T, Keimer B and Ulrich C 2009 *Phys. Rev.* B **80** 064509
[137] Chauviere L, Gallais Y, Cazayous M, Sacuto A, Measson M A, Colson D and Forget A 2009 *Phys. Rev.* B **80** 094504
[138] Singh D and Du M 2008 *Phys. Rev. Lett.* **100** 237003
[139] Boeri L, Dolgov O V and Golubov A A 2008 *Phys. Rev. Lett.* **101** 026403
[140] Mazin I I, Johannes M D, Boeri L, Koepernik K and Singh D J 2008 *Phys. Rev.* B **78** 085104
[141] Fukuda T et al., 2008 *J. Phys. Soc. Japan.* **77** 103715
[142] Christianson A D et al., 2008 *Phys. Rev. Lett.* **101** 157004
[143] Choi K Y, Lemmens P, Eremin I, Zwicknagl G, Berger H, Sun G L, Sun D L and Lin C T 2010 *J. Phys. Cond. Matt* **22** 115802
[144] Delaire O et al., 2010 *Phys. Rev.* B **81** 094504
[145] Zbiri M, Schober H, Johnson M R, Rols S, Mittal R, Su Y, Rotter M and Johrendt D 2009 *Phys. Rev.* B **79** 064511
[146] Mittal R, Rols S, Zbiri M, Su Y, Schober H, Chaplot S L, Johnson M, Tegel M, Chatterji T, Matsuishi S, Hosono H, Johrendt D and Brueckel T 2009 *Phys. Rev.* B **79** 144516
[147] Mittal R, Zbiri M, Rols S, Su Y, Xiao Y, Schober H, Chaplot S L, Johnson M, Chatterji T, Matsuishi S, Hosono H and Brueckel T 2009 *Phys. Rev.* B **79** 214514
[148] Huang Q, Qiu Y, Bao W, Green M A, Lynn J W, Gasparovic Y C, Wu T, Wu G, and Chen X H 2008 *Phys. Rev. Lett.* **101** 257003
[149] Yildirim T 2009 *Physica. C* **469** 425
[150] Goldman A I, Argyriou D N, Ouladdiaf B, Chatterji T, Kreyssig A, Nandi S, Ni N, Bud'ko S L, Canfield P C and McQueeney R J 2008 *Phys. Rev.* B **78** 100506
[151] Lebègue S, Yin Z P and Pickett W E 2009 *New J. Phys.* **11** 025004
[152] Kasinathan D, Ormeci A, Koch K, Burkhardt U, Schnelle W, Leithe-Jasper A and Rosner H 2009 *New J. Phys.* **11** 025023
[153] Parlinski K, Li Z Q and Kawazoe Y 1997 *Phys. Rev. Lett.* **78** 4063
[154] Parlinksi K Software phonon and 2003